
Bayesian Nonparametric Mixed-Effect ODEs with Gaussian Processes

Julien Martinelli* Maksim Sinelnikov Harri Lähdesmäki

Aalto University

Quentin Clairon† Mélanie Prague†

Univ. Bordeaux, INSERM BPH, U1219, Inria SISTM team, VRI, France

Abstract

Dynamical modelling is central to many scientific domains, including pharmacometrics, systems biology, physiology, and epidemiology. In these settings, heterogeneity is often intrinsic: different subjects or units follow related but distinct continuous-time dynamics. Classical nonlinear mixed-effects Ordinary Differential Equation (ODE) models address this by combining population-level structure with subject-specific effects, but they rely on a parametric vector field and are therefore vulnerable to structural misspecification and unmodelled mechanisms. This motivates nonparametric approaches that can retain principled uncertainty quantification, yet existing nonparametric ODE methods typically assume a single shared dynamical system rather than an explicit mixed-effect hierarchy over subject-specific dynamics. We propose MEGPODE, a Bayesian nonparametric mixed-effect ODE model in which each subject’s vector field is decomposed into a shared population component and a subject-specific deviation, both endowed with Gaussian process (GP) priors. To avoid repeated ODE solves per subject during training, we combine state-space GP trajectory priors with virtual collocation observations, yielding Kalman-smoothing trajectory updates and closed-form regressions for the vector fields. Across controlled heterogeneous ODE benchmarks spanning oscillatory, biomedical systems, MEGPODE improves population-field recovery and subject-level trajectory prediction relative to strong baselines.

1 Introduction

Ordinary differential equation (ODE) models are a standard language for mechanistic modeling in systems biology, medicine, vaccinology, and pharmacometrics because they encode interpretable dynamics and support extrapolation beyond the observed window [24]. In longitudinal population studies, however, the scientific object is rarely a single trajectory. Different patients, cells, or experimental units often follow related but distinct dynamical laws, and the practical question is how to model that heterogeneity in a statistically efficient way [1, 8].

The classical framework for this setting is nonlinear mixed-effects (NLME) ODE modelling, where a shared mechanistic system is coupled with subject-specific random effects [18]. This is appealing because heterogeneity is represented at the level of the *dynamics* rather than only at the *trajectory* level. But it is also restrictive: one must commit to a parametric vector field and to a specific low-dimensional random-effect parameterization. This can be problematic in the very regimes where these models are most often used, for instance in biology, medicine, and pharmacometrics [25]. There, mechanisms are often only partially known, individual differences may not be well captured by a few

*Work initiated while at the Inria SISTM team.

†Equal contribution in supervision.

parameter perturbations, and observations are typically noisy, sparse, and irregularly sampled. In such settings, parametric NLME-ODEs can be misspecified and difficult to fit [20].

These limitations point toward nonparametric dynamics modelling. Flexible continuous-time models based on Gaussian processes (GPs) or neural ODEs can learn unknown dynamics without committing to a detailed mechanistic family [6, 13–16, 22, 41]. But most of this literature is built for a single shared dynamical system rather than a heterogeneous population. Conversely, recent population-level continuous-time models do capture subject variability, yet typically through finite-dimensional parametric or neural effects rather than a Bayesian nonparametric hierarchy over subject-specific vector fields [2, 5, 20, 27, 28]. This leaves a clear methodological gap: we still lack a nonparametric mixed-effect model for continuous-time dynamics that operates directly at the ODE level and provides uncertainty quantification at both the population and subject levels.

Contributions. We introduce MEGPODE, a Bayesian nonparametric mixed-effect ODE model. Figure 1 summarizes the method, Table 1 positions it against related work. Our contributions are:

- **Conceptual:** we introduce a nonparametric mixed-effect formulation for ODE dynamics, translating the classical NLME decomposition between population-level and individual-level effects from parameter space to function space.
- **Methodological:** we develop an inference scheme that combines state-space GP trajectory priors with collocation-based ODE constraints, yielding Kalman-smoothing updates for latent trajectories and scalable Gaussian updates for shared and subject-specific vector fields.
- **Empirical:** we evaluate MEGPODE on diverse controlled heterogeneous ODE benchmarks, assessing population-field recovery, forecasting, and uncertainty quantification, showing consistent improvements over strong baselines.
- **Theoretical:** we derive computable diagnostics for uncertainty and complexity under the mixed-effect field decomposition.

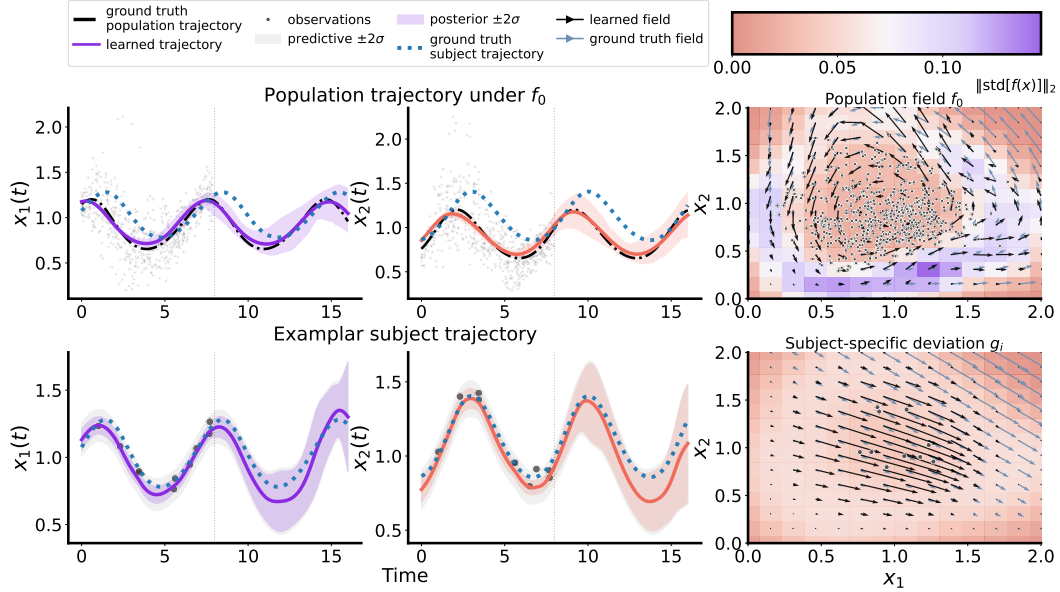


Figure 1: **Overview of our method.** Learned shared and subject-specific dynamics on a 2D system. The top-row trajectory panels show the population trajectory induced by the shared field f_0 , with bands denoting uncertainty in the *population trajectory*; the blue curve shows the ground-truth trajectory of a subject whose trajectory deviates substantially from the population trajectory. Bottom-row panels show the posterior trajectory of this subject. Dots denote observations ($M = 30$ subjects in the population panels, each with 10 observations). The right-column panels show the learned and ground-truth shared field f_0 and subject-specific deviation g_i in state space. The colormap shows predictive uncertainty magnitude.

	Personalized	Flexible dynamics	Mixed-effect	Probabilistic
Parametric NLME-ODEs [39]	✓	✗	✓	✓
Mixed-Effect GPs [7, 19, 42]	✓	✗	✓	✓
GP-ODEs [13, 15, 22]	✗	✓	✗	✓
Mixed-effects Neural ODEs [27]	✓	✓ (latent)	≈ (non additive)	✓
Contextual neural dynamics [12, 17, 26]	✓	✓	✗	✗
MEGPODE (This work)	✓	✓	✓	✓

Table 1: Comparison with related work. **MEGPODE is designed to do what prior approaches only partially cover: learn flexible probabilistic population dynamics and personalize them via an explicit subject-specific mixed-effect field.**

2 Background

2.1 Problem setup

We observe M subjects. Subject i is measured at times $\mathcal{T}_i = \{t_{i,1} < \dots < t_{i,N_i}\}$, with observations $\mathbf{y}_{i,n} \in \mathbb{R}^{D_y}$. Let $\mathbf{x}_i(t) \in \mathbb{R}^D$ denote the latent dynamical state. We assume a linear-Gaussian observation model

$$\mathbf{y}_{i,n} \mid \mathbf{x}_i(t_{i,n}) \sim \mathcal{N}(\mathbf{H}\mathbf{x}_i(t_{i,n}), \boldsymbol{\Sigma}_y), \quad \mathbf{H} \in \mathbb{R}^{D_y \times D}, \quad (1)$$

and a subject-specific ODE

$$\dot{\mathbf{x}}_i(t) = \mathbf{f}_i(\mathbf{x}_i(t)), \quad \mathbf{x}_i(t_{i,0}) = \mathbf{x}_{i,0}. \quad (2)$$

The learning problem is to recover a collection of related subject-level vector fields from irregular and partially observed longitudinal data. In the spirit of mixed-effects modeling, we seek a decomposition of subject dynamics into a shared population component and a subject-specific deviation; the explicit form of that decomposition is introduced in Section 3.1. We next review the GP and state-space ingredients that make this construction computationally tractable.

2.2 Gaussian processes and state-space trajectory priors

A convenient probabilistic starting point for continuous-time trajectories is the GP [30]. Writing

$$f \sim \mathcal{GP}(m, k), \quad (3)$$

means that any finite collection of function values is jointly Gaussian, with mean function m and covariance kernel k . For differentiable kernels, derivatives are jointly Gaussian with function values as well, since differentiation is a linear operator. This makes GPs a natural tool when both a trajectory and its derivative matter.

For temporal modelling, an important subclass of GP priors admits an equivalent state-space representation. In particular, Matérn kernels and integrated Wiener-process priors can be written as linear stochastic differential equations whose discretization on an irregular grid $\tau_{0:K}$ yields a Gaussian Markov chain [33, 38, 43]:

$$\mathbf{s}_{k+1} = \mathbf{A}(h_k)\mathbf{s}_k + \mathbf{q}_k, \quad \mathbf{q}_k \sim \mathcal{N}(\mathbf{0}, \mathbf{Q}(h_k)), \quad h_k = \tau_{k+1} - \tau_k, \quad (4)$$

for a suitable latent state \mathbf{s}_k . Under linear-Gaussian observations, posterior inference then scales linearly in the grid size K through Kalman filtering and smoothing [32].

To keep both the state and its derivative explicit, define the latent state at time $\tau_{i,k}$ as

$$\mathbf{s}_{i,k} := \begin{bmatrix} \mathbf{x}_i(\tau_{i,k}) \\ \dot{\mathbf{x}}_i(\tau_{i,k}) \end{bmatrix} \in \mathbb{R}^{2D}, \quad \mathbf{x}_i(\tau_{i,k}) = \mathbf{H}_x \mathbf{s}_{i,k}, \quad \dot{\mathbf{x}}_i(\tau_{i,k}) = \mathbf{H}_x \mathbf{s}_{i,k}, \quad (5)$$

with $\mathbf{H}_x = [\mathbf{I}_D \ \mathbf{0}_{D \times D}] \in \mathbb{R}^{D \times 2D}$ and $\mathbf{H}_x = [\mathbf{0}_{D \times D} \ \mathbf{I}_D] \in \mathbb{R}^{D \times 2D}$. For example, an integrated Wiener-process prior of order two yields $\mathbf{A}(h) = \begin{bmatrix} 1 & h \\ 0 & 1 \end{bmatrix} \otimes \mathbf{I}_D \in \mathbb{R}^{2D \times 2D}$ together with a matching process covariance $\mathbf{Q}(h) = \sigma_{\text{IWP}}^2 \begin{bmatrix} h^3/3 & h^2/2 \\ h^2/2 & h \end{bmatrix} \otimes \mathbf{I}_D \in \mathbb{R}^{2D \times 2D}$. The resulting prior is Gaussian and Markov on irregular subject-specific grids, while keeping both trajectories and derivatives available for the ODE construction introduced next.

2.3 Soft ODE constraints via virtual observations

To connect the trajectory prior with the ODE, the dynamical relation is imposed as a soft constraint rather than through repeated numerical integration. Given a known vector field \mathbf{f} , one may require at *collocation times* $\tau_{i,k}$ that the state derivative agrees with the ODE up to a small collocation error:

$$\mathbf{0} = \mathbf{H}_{\dot{\mathbf{x}}}\mathbf{s}_{i,k} - \mathbf{f}(\mathbf{H}_x\mathbf{s}_{i,k}) + \boldsymbol{\epsilon}_{i,k}^{(\text{coloc})}, \quad \boldsymbol{\epsilon}_{i,k}^{(\text{coloc})} \sim \mathcal{N}(\mathbf{0}, \boldsymbol{\Sigma}_{\text{coloc}}). \quad (6)$$

This construction was proposed by [13, 22]. After local linearization, this becomes a Gaussian pseudo-observation on $\mathbf{s}_{i,k}$, so the resulting posterior remains a Gauss–Markov smoothing problem. Section 3.3 extends this construction to the case where the field \mathbf{f} is itself unknown and hierarchical.

3 Mixed-effect Gaussian Process ODEs (MEGPODE)

We now present our method. Section 3.1 introduces the mixed-effect GP prior over subject-specific fields. Section 3.2 describes the scalable representation used for the shared and local fields. Section 3.3 explains the trajectory-space update obtained by locally linearizing the collocation factor inside a state-space GP prior. Section 3.4 turns smoothed trajectories into a heteroscedastic mixed regression problem that updates shared and local fields. Algorithm 1 summarizes the full loop.

3.1 Hierarchical GP prior on subject-specific vector fields

We model each subject-specific field as the sum of a population field and an individual deviation,

$$\mathbf{f}_i(\mathbf{x}) = \mathbf{f}_0(\mathbf{x}) + \mathbf{g}_i(\mathbf{x}), \quad i = 1, \dots, M. \quad (7)$$

We use independent-output GP priors across state dimensions $d = 1, \dots, D$:

$$f_{0,d}(\cdot) \sim \mathcal{GP}(0, k_0), \quad f_{0,d} \perp f_{0,d'} \text{ for } d \neq d', \quad (8)$$

$$g_{i,d}(\cdot) \sim \mathcal{GP}(0, k_r), \quad g_{i,d} \perp g_{j,d'} \text{ for } (i, d) \neq (j, d'), \quad i = 1, \dots, M. \quad (9)$$

It follows that, for any inputs \mathbf{x}, \mathbf{x}' ,

$$\text{Cov}[f_{i,d}(\mathbf{x}), f_{j,d'}(\mathbf{x}')] = \mathbb{I}[d = d'] (k_0(\mathbf{x}, \mathbf{x}') + \mathbb{I}[i = j]k_r(\mathbf{x}, \mathbf{x}')). \quad (10)$$

Thus all subjects borrow strength through the common field, which is exactly the classical NLME philosophy translated from parameter space to function space. MAGMA provides a closely related common-mean construction for trajectory regression [19]; here the common component acts directly on the vector field. Even though the prior factorizes across output dimensions, the dimensions will be coupled again by the state-space dynamics and collocation constraints during trajectory inference.

3.2 Scalable representation of shared and local vector fields

Direct GP inference over all field evaluations is expensive. To obtain a scalable approximation, the shared and subject-specific fields are represented via separate inducing-feature expansions. Let $\mathbf{Z}_0 \in \mathbb{R}^{l_0 \times D}$ and $\mathbf{Z}_r \in \mathbb{R}^{l_r \times D}$ denote the inducing locations for the population and residual fields, with l_0 and l_r the corresponding numbers of inducing points. Using the associated kernel Gram matrices to whiten the basis, define the feature maps

$$\Phi_0(\mathbf{x}) = k_0(\mathbf{x}, \mathbf{Z}_0)k_0(\mathbf{Z}_0, \mathbf{Z}_0)^{-1/2} \in \mathbb{R}^{1 \times l_0}, \quad \Phi_r(\mathbf{x}) = k_r(\mathbf{x}, \mathbf{Z}_r)k_r(\mathbf{Z}_r, \mathbf{Z}_r)^{-1/2} \in \mathbb{R}^{1 \times l_r}. \quad (11)$$

For each output dimension d , we approximate

$$f_{0,d}(\mathbf{x}) \approx \Phi_0(\mathbf{x})\mathbf{b}_{0,d}, \quad g_{i,d}(\mathbf{x}) \approx \Phi_r(\mathbf{x})\mathbf{b}_{i,d}, \quad (12)$$

with Gaussian coefficient priors

$$\mathbf{b}_{0,d} \sim \mathcal{N}(\mathbf{0}, \mathbf{I}_{l_0}), \quad \mathbf{b}_{i,d} \sim \mathcal{N}(\mathbf{0}, \lambda_r^{-1}\mathbf{I}_{l_r}). \quad (13)$$

The shrinkage parameter λ_r controls the magnitude of the subject-specific field. $\lambda_r > 1$ increases regularization of individual deviations, shifting explanatory power toward the shared population field.

We maintain Gaussian posteriors $q(\mathbf{b}_{0,d}) = \mathcal{N}(\mathbf{m}_{0,d}, \mathbf{S}_{0,d})$ and $q(\mathbf{b}_{i,d}) = \mathcal{N}(\mathbf{m}_{i,d}, \mathbf{S}_{i,d})$. Conditional on a fixed input \mathbf{x} , the model for the latent subject-specific field value $f_{i,d}(\mathbf{x})$ is linear-Gaussian in these coefficients. Its predictive mean and variance are thus available in closed form:

$$\mu_{i,d}^f(\mathbf{x}) = \Phi_0(\mathbf{x})\mathbf{m}_{0,d} + \Phi_r(\mathbf{x})\mathbf{m}_{i,d}, \quad v_{i,d}^f(\mathbf{x}) = \Phi_0(\mathbf{x})\mathbf{S}_{0,d}\Phi_0(\mathbf{x})^\top + \Phi_r(\mathbf{x})\mathbf{S}_{i,d}\Phi_r(\mathbf{x})^\top. \quad (14)$$

Likewise, the Jacobian of the posterior-mean field is explicit because the feature maps are differentiable. The main challenge lies not in evaluating field moments at a fixed state, but in handling uncertainty in the latent trajectory itself. The next two subsections resolve this by alternating between trajectory smoothing and field regression.

3.3 Trajectory-space inference via local collocation linearization

Naively maximizing a likelihood based on the unknown subject fields would require repeatedly solving one nonlinear ODE per subject every time the shared or local field changes. We avoid this by introducing an auxiliary trajectory posterior on a subject-specific collocation grid $\mathcal{C}_i := \{\tau_{i,0}, \dots, \tau_{i,K_i}\}$ that contains the observation times. We use a mean-field variational factorization

$$q(\{\mathbf{b}_{0,d}\}, \{\mathbf{b}_{i,d}\}, \{\mathbf{s}_{i,0:K_i}\}) = \left(\prod_{d=1}^D q(\mathbf{b}_{0,d}) \right) \left(\prod_{i=1}^M \prod_{d=1}^D q(\mathbf{b}_{i,d}) \right) \left(\prod_{i=1}^M q(\mathbf{s}_{i,0:K_i}) \right), \quad (15)$$

where $q(\mathbf{s}_{i,0:K_i})$ denotes the variational posterior over the latent trajectory of subject i on \mathcal{C}_i . The initial state $\mathbf{x}_{i,0}$ is treated as a latent subject-specific quantity and modeled through a mixed-effect Gaussian decomposition. Details are provided in Appendix D.5.

Following Section 2.3, collocation is imposed via soft pseudo observations. Here, however, the field is both subject-specific and unknown. For subject i and collocation index k , the ODE residual is

$$\mathbf{0} = \mathbf{H}_{\dot{\mathbf{x}}} \mathbf{s}_{i,k} - \mathbf{f}_i(\mathbf{H}_x \mathbf{s}_{i,k}) + \boldsymbol{\epsilon}_{i,k}^{(\text{coloc})}, \quad \boldsymbol{\epsilon}_{i,k}^{(\text{coloc})} \sim \mathcal{N}(\mathbf{0}, \boldsymbol{\Sigma}_{\text{coloc}}). \quad (16)$$

This term is difficult to handle for two reasons: $\mathbf{f}_i(\mathbf{H}_x \mathbf{s}_{i,k})$ is a nonlinear function of the latent state, and the vector field itself remains uncertain under the current posterior. We therefore approximate $\mathbf{f}_i(\mathbf{H}_x \mathbf{s}_{i,k})$ locally by a Gaussian distribution around a reference point $\bar{\mathbf{x}}_{i,k}$ from the previous trajectory iterate. Its mean is given by a first-order expansion of the posterior-mean vector field, while its covariance captures posterior uncertainty in the field evaluation. Define

$$\boldsymbol{\mu}_{i,k}^f = \mathbb{E}_q[\mathbf{f}_i(\bar{\mathbf{x}}_{i,k})], \quad \boldsymbol{\Sigma}_{i,k}^f = \text{Var}_q[\mathbf{f}_i(\bar{\mathbf{x}}_{i,k})], \quad \mathbf{J}_{i,k} = \nabla_{\mathbf{x}} \mathbb{E}_q[\mathbf{f}_i(\mathbf{x})] \Big|_{\mathbf{x}=\bar{\mathbf{x}}_{i,k}}. \quad (17)$$

A first-order expansion of the posterior-mean field then gives

$$\mathbb{E}_q[\mathbf{f}_i(\mathbf{H}_x \mathbf{s}_{i,k})] \approx \boldsymbol{\mu}_{i,k}^f + \mathbf{J}_{i,k}(\mathbf{H}_x \mathbf{s}_{i,k} - \bar{\mathbf{x}}_{i,k}), \quad (18)$$

and this leads to the Gaussian pseudo-observation

$$\mathbf{c}_{i,k}^{(\text{coloc})} = \mathbf{H}_{i,k}^{(\text{coloc})} \mathbf{s}_{i,k} + \boldsymbol{\epsilon}_{i,k}, \quad \boldsymbol{\epsilon}_{i,k} \sim \mathcal{N}(\mathbf{0}, \mathbf{R}_{i,k}^{(\text{coloc})}), \quad \text{and} \quad (19)$$

$$\mathbf{H}_{i,k}^{(\text{coloc})} = \mathbf{H}_{\dot{\mathbf{x}}} - \mathbf{J}_{i,k} \mathbf{H}_x, \quad \mathbf{c}_{i,k}^{(\text{coloc})} = \boldsymbol{\mu}_{i,k}^f - \mathbf{J}_{i,k} \bar{\mathbf{x}}_{i,k}, \quad \mathbf{R}_{i,k}^{(\text{coloc})} = \boldsymbol{\Sigma}_{\text{coloc}} + \boldsymbol{\Sigma}_{i,k}^f. \quad (20)$$

$\mathbf{H}_{i,k}^{(\text{coloc})}$ is the local linearized ODE-residual operator: it maps the augmented state $\mathbf{s}_{i,k}$ to the difference between the derivative component $\dot{\mathbf{x}}_{i,k}$ and the Jacobian-linearized field evaluation at $\mathbf{x}_{i,k}$. The derivation is given in Appendix D.1.

The observation model in Eq. (1), the state-space prior in Eq. (4), and the collocation pseudo-observation in Eq. (19) together define a linear-Gaussian smoothing problem. Therefore, each $q(\mathbf{s}_{i,0:K_i})$ is a Gauss–Markov posterior that can be computed by Kalman smoothing. (Appendix D.2). Lastly, as mentioned previously, output coupling arises even if vector-field prior factorizes across output dimensions, as made explicit by the Jacobian $\mathbf{J}_{i,k}$ acting on the augmented state.

3.4 Vector field update as mixed regression on smoothed pseudo-derivatives

After smoothing subject i , we extract pseudo-observations for the vector field:

$$\tilde{\mathbf{x}}_{i,k} = \mathbb{E}_q[\mathbf{x}_i(\tau_{i,k})], \quad \tilde{\dot{\mathbf{x}}}_{i,k} = \mathbb{E}_q[\dot{\mathbf{x}}_i(\tau_{i,k})], \quad \tilde{\mathbf{R}}_{i,k} = \text{Var}_q(\dot{\mathbf{x}}_i(\tau_{i,k})) + \boldsymbol{\Sigma}_{\text{coloc}}. \quad (21)$$

Note that $\tilde{\mathbf{x}}_{i,k}$ differs from $\bar{\mathbf{x}}_{i,k}$: $\bar{\mathbf{x}}_{i,k}$ is the reference point used to construct the local linearization in the current trajectory update, whereas $\tilde{\mathbf{x}}_{i,k}$ is the resulting updated smoothed mean after that update.

Fix an output dimension d . Stack the pseudo-derivative means for subject i as

$$\mathbf{u}_{i,d} = [\tilde{\dot{x}}_{i,0,d}, \dots, \tilde{\dot{x}}_{i,K_i,d}]^\top \in \mathbb{R}^{K_i+1}, \quad (22)$$

and define feature design matrices

$$\mathbf{P}_{0,i,d} = [\Phi_0(\tilde{\mathbf{x}}_{i,j-1})]_{j=1}^{K_i+1} \in \mathbb{R}^{(K_i+1) \times l_0}, \quad \mathbf{P}_{r,i,d} = [\Phi_r(\tilde{\mathbf{x}}_{i,j-1})]_{j=1}^{K_i+1} \in \mathbb{R}^{(K_i+1) \times l_r}. \quad (23)$$

Let $\varepsilon_{i,d}^{\text{reg}} \sim \mathcal{N}(\mathbf{0}, \mathbf{R}_{i,d})$, where $\tilde{\mathbf{R}}_{i,k} \in \mathbb{R}^{D \times D}$ is the local pseudo-derivative covariance at time $\tau_{i,k}$ (Eq. (21)), and $\mathbf{R}_{i,d} \in \mathbb{R}^{(K_i+1) \times (K_i+1)}$ collects the uncertainty for output dimension d across the collocation times, e.g., through the diagonal approximation $\mathbf{R}_{i,d} = \text{diag}([\tilde{\mathbf{R}}_{i,0}]_{dd}, \dots, [\tilde{\mathbf{R}}_{i,K_i}]_{dd})$, or via other conservative variants (Appendix D.7). With this notation, the pseudo-data induce, for each subject i and output dimension d , the heteroscedastic linear-Gaussian mixed regression

$$\mathbf{u}_{i,d} = \mathbf{P}_{0,i,d} \mathbf{b}_{0,d} + \mathbf{P}_{r,i,d} \mathbf{b}_{i,d} + \varepsilon_{i,d}^{\text{reg}}. \quad (24)$$

Thus the field-learning step can be viewed as mixed regression in feature space. Writing Gaussian posterior over a generic coefficient vector \mathbf{b} in natural form,

$$q(\mathbf{b}) \propto \exp\left(-\frac{1}{2} \mathbf{b}^\top \boldsymbol{\Lambda} \mathbf{b} + \boldsymbol{\eta}^\top \mathbf{b}\right),$$

the coefficient updates are obtained by alternating between the shared and local components, each time holding the current posterior mean of the other component fixed. For the shared field,

$$\boldsymbol{\Lambda}_{0,d}^{\text{new}} = \mathbf{I}_{l_0} + \sum_{i=1}^M \mathbf{P}_{0,i,d}^\top \mathbf{R}_{i,d}^{-1} \mathbf{P}_{0,i,d}, \quad (25)$$

$$\boldsymbol{\eta}_{0,d}^{\text{new}} = \sum_{i=1}^M \mathbf{P}_{0,i,d}^\top \mathbf{R}_{i,d}^{-1} (\mathbf{u}_{i,d} - \mathbf{P}_{r,i,d} \mathbf{m}_{i,d}), \quad (26)$$

and for the local field of subject i ,

$$\boldsymbol{\Lambda}_{i,d}^{\text{new}} = \lambda_r \mathbf{I}_{l_r} + \mathbf{P}_{r,i,d}^\top \mathbf{R}_{i,d}^{-1} \mathbf{P}_{r,i,d}, \quad (27)$$

$$\boldsymbol{\eta}_{i,d}^{\text{new}} = \mathbf{P}_{r,i,d}^\top \mathbf{R}_{i,d}^{-1} (\mathbf{u}_{i,d} - \mathbf{P}_{0,i,d} \mathbf{m}_{0,d}). \quad (28)$$

Algorithm 1 summarizes the overall procedure. The same inference scheme yields two downstream procedures: extrapolation for a trained subject, by freezing the learned field posterior and resmoothing on an extended grid (Appendix D.3), and adaptation for a new subject, by freezing the shared posterior and updating only the new subject’s local posterior and trajectory (Appendix D.4). Model hyperparameters are learned via Empirical Bayes after the current smoothing pass (Appendix D.6).

Algorithm 1 Alternating inference for MEGPODE

Require: Kernels k_0, k_r , inducing locations $\mathbf{Z}_0, \mathbf{Z}_r$, a state-space trajectory prior (Section 2.2), and collocation grids containing the observation times.

- 1: Initialize natural parameters $\boldsymbol{\Lambda}_{0,d} = \mathbf{I}_{l_0}$, $\boldsymbol{\eta}_{0,d} = \mathbf{0}$, and $\boldsymbol{\Lambda}_{i,d} = \lambda_r \mathbf{I}_{l_r}$, $\boldsymbol{\eta}_{i,d} = \mathbf{0}$.
 - 2: Initialize subject-specific reference points by $\tilde{\mathbf{x}}_{i,k}^{(0)} = \mathbf{H}_x \mathbb{E} \left[\mathbf{s}_{i,k} \mid \{\mathbf{y}_{i,n}\}_{n=1}^{N_i} \right]$.
 - 3: **Repeat until convergence:**
 - 4: **for** each subject i **do** //parallelizable
 - 5: Evaluate local field moments and Jacobians at $\tilde{\mathbf{x}}_{i,k}$ using Eqs. (14) and (17).
 - 6: Form collocation pseudo-observations (Eqs. (19)–(20)).
 - 7: Update $q(\mathbf{s}_{i,0:K_i})$ by Kalman smoothing (Appendix D.2).
 - 8: Update the mixed-effect initial-condition from smoothed marginals (Appendix D.5).
 - 9: Extract pseudo-observations $(\tilde{\mathbf{x}}_{i,k}, \tilde{\tilde{\mathbf{x}}}_{i,k}, \tilde{\mathbf{R}}_{i,k})$ using Eq. (21), and set $\tilde{\mathbf{x}}_{i,k} \leftarrow \tilde{\tilde{\mathbf{x}}}_{i,k}$.
 - 10: **end for**
 - 11: Build the feature regression problems in Eqs. (22)–(24).
 - 12: Update the shared-field posterior using the natural-parameter updates in Eqs. (25)–(26).
 - 13: Update each local-field posterior using Eqs. (27)–(28).
-

3.5 Structural analysis and representation variants

Structural properties. Appendix E develops structural properties of MEGPODE, summarized in Table S5: well-posed posterior-mean dynamics, population/local covariance and variance decompositions, and the Gaussian geometry of the conditional field update. Two consequences are especially relevant here. First, conditional on the current smoothed pseudo-data, the field update is a strictly convex weighted mixed-ridge regression with a unique minimizer, yielding conditional identifiability of the shared and local components (Proposition 6, Corollary 7). Second, Eq. (25) shows that shared

precision accumulates as a sum of positive semidefinite subject-specific contributions, so adding subjects can only increase shared precision and reduce shared posterior covariance (Proposition 10). This property makes our approach the dynamical analogue of common-mean GPs like MAGMA [19].

Representation variants. Appendix F shows that the method extends beyond inducing features to any finite-dimensional linear-Gaussian field representation with tractable moments and Jacobians, e.g., random Fourier features [29] and Hilbert bases [35]. Appendix D.9 describes an extension where the local coefficients are correlated across subjects via a covariate kernel later used in experiments.

4 Related work

Flexible continuous-time dynamics. GP-ODEs and neural ODE models form the closest continuous-time modelling lineage to our approach. GP-based ODE learning spans nonparametric vector-field inference [15], gradient matching [11, 23, 40], manifold-constrained GP inference [41], variational multiple shooting [14], and collocation-based physics-informed models [13, 22]. Neural ODEs [6], latent ODEs [31], and Neural CDEs [16] provide flexible alternatives for irregular-time prediction and forecasting. These methods learn expressive dynamics, but most assume a single shared dynamical system rather than a population of subject-specific vector fields.

Personalized neural dynamics. Recent approaches adapt continuous-time neural dynamics across environments or patients. Mixed-effect Neural ODEs [27] introduce subject-specific latent random effects into neural ODEs. Context-conditioned neural dynamics, including CoDA [17], MetaPhysiCa [26], and DIF [12], use context variables or meta-learned representations to personalize dynamics across environments. These approaches are flexible and personalized, but lack a probabilistic treatment of the mixed-effect decomposition of the vector field.

Mixed-effect population models. Parametric NLME-ODEs remain the dominant framework for population dynamics in pharmacometrics and systems biology [18, 21, 39]. Population Kalman filtering [9] and recent amortized or in-context estimators [2, 20, 28] improve scalability, personalization, or inference speed, but still operate in predefined parametric or neural model families. Flexible mixed-effect regression models, including common-mean multi-task GPs such as MAGMA [19] and other mixed-effect GP formulations [7, 42], share information across subjects but do not explicitly model continuous-time dynamics. In contrast, MEGPODE places the mixed-effect hierarchy directly over the vector field, combining personalization, flexible dynamics, and function-space uncertainty.

5 Experiments

We evaluate MEGPODE in controlled population-ODE benchmarks where the ground-truth dynamics are known. Experiments will assess whether the mixed-effect field decomposition improves population-level recovery and prediction, how sensitive the method is to its hyperparameters and data regime choices, and whether function-space residuals can correct a misspecified mechanistic population model. All experiments in this section use synthetic systems, which allows us to evaluate both predictive performance and recovery of the underlying population dynamics.

5.1 Benchmark systems and heterogeneity injection

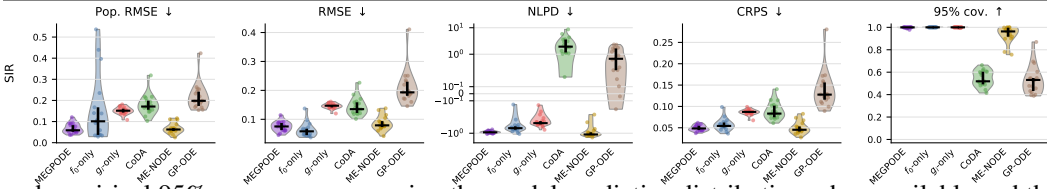
Synthetic benchmark systems. We consider mechanistic population models spanning both oscillatory and non-oscillatory dynamics. The oscillatory benchmarks include a linear oscillator, Lotka–Volterra, Van der Pol, and FitzHugh–Nagumo systems. The non-oscillatory benchmarks include SIR epidemic dynamics and pharmacokinetic models. Subject heterogeneity is introduced through random effects on mechanistic parameters, yielding a direct comparison to baselines that either share one dynamical system or model subject-specific dynamics. Details are given in Appendix C.

Baselines. We compare MEGPODE against GPODE [14], adapted with one shared latent vector field and subject-specific initial states; CoDA [17], which conditions a neural vector field on learned subject codes; and a mixed-effect neural ODE [27]. Details are given in Appendix B.1. We also include two ablations: `f0_only`, which sets $g_i \equiv 0$, and `gi_only`, which sets $f_0 \equiv 0$ (Appendix B.2).

Metrics. We evaluate prediction in interpolation and forecasting settings. At the subject level, we report RMSE, negative log predictive density (NLPD), continuous ranked probability score (CRPS),

Table 2: **Synthetic benchmark performance. Top:** average target-window ranks across synthetic systems. For each system, mode, and metric, methods are ranked after averaging over seeds; entries report mean \pm standard deviation across systems, with lower ranks better. **Bottom:** SIR forecast performance over 20 seeds; full benchmark distributions are shown in Figures S2 and S3. **MEGPODE achieves the strongest average ranks for trajectory accuracy and distributional forecast quality, while remaining competitive on uncertainty calibration.**

Setting	Metric	MEGPODE	f_0 -only	g_i -only	CoDA	ME-NODE	GP-ODE
Forecast	Pop. RMSE rank \downarrow	1.57 \pm 0.79	3.43 \pm 1.51	3.71 \pm 1.11	4.29 \pm 1.60	3.29 \pm 2.14	4.71 \pm 1.50
	RMSE rank \downarrow	2.86 \pm 1.07	4.14 \pm 1.46	3.57 \pm 1.27	3.71 \pm 2.36	<u>3.00 \pm 1.91</u>	3.71 \pm 2.21
	NLPD rank \downarrow	3.43 \pm 1.62	4.29 \pm 1.38	3.86 \pm 1.21	4.43 \pm 2.15	2.29 \pm 1.80	<u>2.71 \pm 1.50</u>
	CRPS rank \downarrow	2.86 \pm 1.35	4.14 \pm 1.21	3.71 \pm 1.11	3.29 \pm 2.29	<u>3.00 \pm 2.16</u>	4.00 \pm 2.08
	95% cov. rank \downarrow	3.57 \pm 1.13	4.14 \pm 1.95	4.00 \pm 1.29	3.14 \pm 1.77	2.86 \pm 2.41	3.29 \pm 1.80
Interpolation	Pop. RMSE rank \downarrow	1.14 \pm 0.38	2.43 \pm 0.98	3.43 \pm 0.79	5.29 \pm 0.49	3.00 \pm 0.82	5.71 \pm 0.49
	RMSE rank \downarrow	1.29 \pm 0.49	<u>2.00 \pm 0.58</u>	3.57 \pm 0.53	3.43 \pm 1.40	4.71 \pm 0.49	6.00 \pm 0.00
	NLPD rank \downarrow	2.86 \pm 2.12	3.14 \pm 1.68	4.00 \pm 1.53	4.14 \pm 1.95	2.57 \pm 1.40	4.29 \pm 1.38
	CRPS rank \downarrow	1.29 \pm 0.49	<u>2.14 \pm 0.69</u>	3.86 \pm 0.69	3.29 \pm 1.50	4.43 \pm 0.79	6.00 \pm 0.00
	95% cov. rank \downarrow	<u>3.29 \pm 1.98</u>	3.57 \pm 1.40	3.86 \pm 1.57	4.29 \pm 1.11	1.57 \pm 1.51	4.43 \pm 1.51



and empirical 95% coverage error, using the model predictive distribution when available and the fitted observation-noise model otherwise. At the population level, we compare the inferred shared trajectory to the known synthetic population trajectory using population RMSE, which directly assesses whether f_0 is recovered in a dynamically meaningful way.

5.2 Results

Table 2 summarizes target-window performance across synthetic benchmarks. For each system, evaluation mode, and metric, we average over seeds, rank methods, and report the mean \pm standard deviation of ranks across systems. This rank-based summary avoids over-weighting systems whose raw metric scales are intrinsically larger. Full per-system distributions displayed in Figures S2–S3.

MEGPODE gives the strongest overall trajectory recovery. It ranks first for population RMSE in both forecasting and interpolation, indicating more accurate recovery f_0 . ME-NODE is often stronger on NLPD and coverage, suggesting more conservative uncertainty estimates, but this advantage comes with a weaker match to the target trajectories: MEGPODE obtains better average RMSE and CRPS ranks. CoDA is competitive on some subject-level tasks but lacks an explicit probabilistic population field, while GP-ODE is probabilistic but uses only one shared field with subject-specific initial conditions. Both therefore miss part of the mixed-effect field hierarchy, which is reflected in weaker population or trajectory metrics. Finally, considering f_0 -only, which removes personalization, and g_i -only, which removes cross-subject borrowing, both generally underperform the full model, indicating that accurate population recovery and individualized forecasting require both f_0 and g_i .

Beyond predictive accuracy, MEGPODE uniquely provides a probabilistic treatment of both the shared field and subject-specific deviations. This enables useful diagnostics for field- and trajectory-level uncertainty decomposition as population and local contributions. Figure S4 illustrates these diagnostics using Equations (S59), (S70), and (S90), formally introduced in Appendices E.2 and E.4.

5.3 Correcting misspecified mechanistic population dynamics

Because mechanistic ODEs often capture only part of the true dynamics, we use an engineered FitzHugh–Nagumo benchmark to test whether function-space mixed effects can correct such incompleteness. We use an engineered FitzHugh–Nagumo benchmark in which

$$f_0^*(x) = f_{\text{FHN}}(x; \theta^*) + h_0(x),$$

where h_0 is a smooth state-dependent correction. Subjects also have smooth residual fields g_i^* (Appendix C.3).

Figure 2 compares three approaches: mechanistic SAEM, which fits the FHN mixed-effect model without residual correction; standard MEGPODE, which learns a fully nonparametric population-

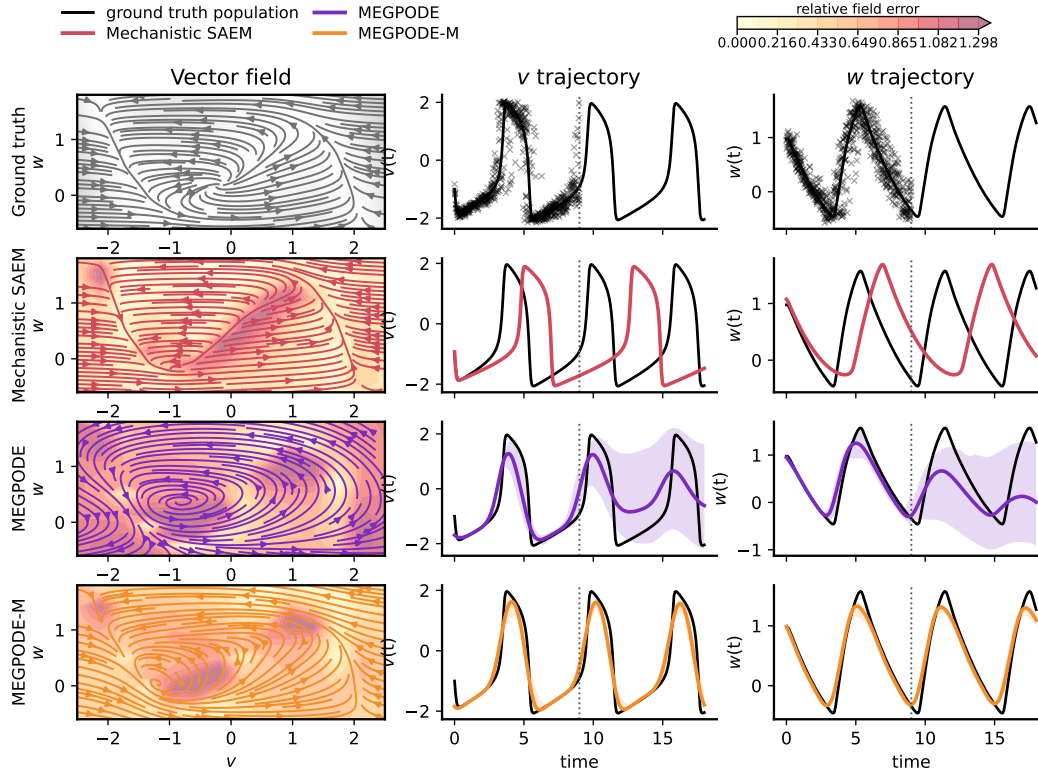


Figure 2: **Misspecified FHN setting.** Population fields and forecasts when the true dynamics include a smooth residual term. **The semi-mechanistic version of MEGPODE best recovers the corrected field and forecast dynamics.**

plus-subject decomposition; and MEGPODE-M, our semi-mechanistic variant with an FHN mean and GP residual (Appendix C.3). The mechanistic fit is constrained by the misspecified FHN family and accumulates phase and amplitude errors in forecast. Standard MEGPODE is flexible, but its population field is weakly constrained away from the observed region in this low-data extrapolation setting. In contrast, MEGPODE-M combines the FHN inductive bias with a function-space residual correction, yielding the closest population field and the most accurate forecasts.

5.4 Ablations

We study sensitivity to model hyperparameters and experimental design by varying one factor at a time around the default configuration. Results are averaged over the main benchmark systems and 10 random seeds. For lower-is-better metrics, we report $\Delta_{\text{rel}} = 100 \frac{\mathcal{M}_{\text{base}} - \mathcal{M}_{\text{abl}}}{|\mathcal{M}_{\text{base}}|}$, with the sign reversed for higher-is-better metrics; thus positive values indicate improvement over the default.

Hyperparameter ablations. We assess the sensitivity of MEGPODE to its main modelling hyperparameters: the integrated-Wiener-process scale σ_{IWP}^2 , the collocation covariance Σ_{coloc} , the collocation-grid size $|\mathcal{C}_i| = K_i + 1$, the residual shrinkage parameter λ_r , and the shared/local inducing capacities (l_0, l_r) . Figure 3 shows that MEGPODE admits a broad basin of good configurations. In forecast mode, the largest degradations occur for too little process noise, too little collocation variance, very coarse collocation grids, and weak residual shrinkage ($\lambda_r = 0.1$), with the population trajectory metric being especially sensitive. At the same time, population RMSE displays a clear interior optimum: moderate σ_{IWP}^2 , moderate Σ_{coloc} , intermediate grid sizes, and moderate λ_r consistently lie in the best region, and the default setting falls close to this basin. The inducing-capacity ablations are asymmetric, with l_0 mattering mainly when it is too small, whereas performance is comparatively flat once l_r is moderately large. Interpolation follows the same overall pattern, but the best region shifts toward slightly larger σ_{IWP}^2 and Σ_{coloc} , and toward somewhat smaller collocation grids (Figure S5).

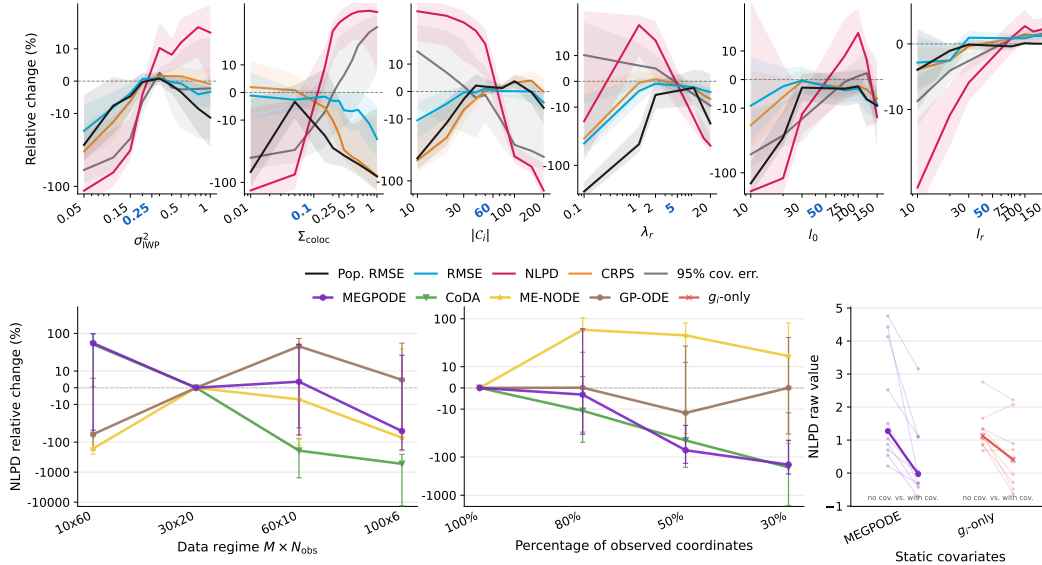


Figure 3: **Ablations for MEGPODE (forecast setting).** **Top:** hyperparameter ablations. Each panel varies a single hyperparameter around the default configuration, while keeping the rest of the training and evaluation pipeline fixed; the blue tick marks the default value. Mean ± 0.5 std relative change with respect to the default setting shown, averaged over 10 seeds and the benchmark systems used in the ablation study. **Bottom:** ablations on the experimental setting.

Experimental-setting ablations. We vary the data regime and observation structure while keeping the model class fixed (Figure 3, bottom). MEGPODE and CoDA benefit from denser individual trajectories, GP-ODE from more subjects with fewer observations, and ME-NODE is comparatively less sensitive. Next, as expected, reducing the fraction of observed state coordinates in every sample generally degrades performance, although ME-NODE shows a less regular trend. Finally, on the Lotka–Volterra covariate benchmark (Appendix C.2), our static covariate extension (Appendix D.9) reduces the paired raw NLPD relative to its non-covariate counterpart, supporting covariate kernels as a way to share information across subjects with similar static attributes.

6 Discussion

We introduced MEGPODE, a flexible mixed-effect model for heterogeneous continuous-time dynamics. By decomposing each subject’s vector field with GP priors over both the population field and subject-specific deviations, MEGPODE lifts the classical NLME-ODE population/individual decomposition from parameter space to vector-field function space. At the same time, it can be seen as the dynamical analogue of mixed-effect GPs [19]: the shared and local components act on the ODE drift rather than directly on trajectories or regression outputs. Our approach combines state-space collocation with Kalman smoothing trajectory inference without repeated ODE solves.

Limitations. Our empirical study is limited to synthetic examples; while this enables ground-truth evaluation of fields and population trajectories, validation on real-world longitudinal data remains a key next step. Next, MEGPODE depends on kernel and scalable representation choices. We use inducing features, but any differentiable finite-dimensional linear-Gaussian field representation can be used (Appendix F). Finally, the trajectory update relies on local linearization of the nonlinear collocation factor, so accuracy may degrade when the state posterior is broad or strongly multimodal.

Perspectives. A key direction is to develop *grey-box* extensions [34, 36, 44]. Motivated by Section 5.3, MEGPODE could combine a mechanistic ODE backbone with GP residual fields, correcting structural misspecification while separating parametric dynamics from residual uncertainty. A second direction is to move from static subject covariates to *dynamical covariates*, enabling more faithful modelling of biomedical trajectories driven by time-varying inputs. These directions mirror a broader

biology-informed ML perspective: combining mechanistic structure, subject-level context, and flexible data-driven components rather than relying on any single source of information [25].

References

- [1] Marie Alexandre, Mélanie Prague, Chelsea McLean, Viki Bockstal, Macaya Douougih, Rodolphe Thiébaud, Thierry Effelterre, Laura Solforosi, and Anna Dari. Prediction of long-term humoral response induced by the two-dose heterologous ad26.zebov, mva-bn-filo vaccine against ebola. *npj Vaccines*, 2023.
- [2] Jonas Arruda, Yannik Schälte, Clemens Peiter, Olga Teplytska, Ulrich Jaehde, and Jan Hase-nauer. An amortized approach to non-linear mixed-effects modeling based on neural posterior estimation. In *Proceedings of the 41st International Conference on Machine Learning*, 2024.
- [3] Christopher M Bishop and Nasser M Nasrabadi. *Pattern recognition and machine learning*. Springer, 2006.
- [4] Stephen Boyd and Lieven Vandenberghe. *Convex Optimization*. Cambridge University Press, 2004.
- [5] Dominic Stefan Bräm, Bernhard Steiert, Marc Pfister, Britta Steffens, and Gilbert Koch. Low-dimensional neural ordinary differential equations accounting for inter-individual variability implemented in monolix and nonmem. *CPT: Pharmacometrics & Systems Pharmacology*, 2025.
- [6] Ricky T. Q. Chen, Yulia Rubanova, Jesse Bettencourt, and David Duvenaud. Neural ordinary differential equations. In *Advances in Neural Information Processing Systems*, 2018.
- [7] Ingyo Chung, Saehoon Kim, Juho Lee, Kwang Joon Kim, Sung Ju Hwang, and Eunho Yang. Deep mixed effect model using gaussian processes: A personalized and reliable prediction for healthcare. *Proceedings of the AAAI Conference on Artificial Intelligence*, 2020.
- [8] Quentin Clairon, Mélanie Prague, Delphine Planas, Timothée Bruel, Laurent Hocqueloux, Thierry Prazuck, Olivier Schwartz, Rodolphe Thiébaud, and Jérémie Guedj. Modeling the kinetics of the neutralizing antibody response against sars-cov-2 variants after several administrations of bnt162b2. *PLoS Computational Biology*, 2023.
- [9] Annabelle Collin, Mélanie Prague, and Philippe Moireau. Estimation for dynamical systems using a population-based kalman filter—applications in computational biology. *MathematicS In Action*, 2022.
- [10] Emmanuelle Comets, Audrey Lavenu, and Marc Lavielle. Parameter estimation in nonlinear mixed effect models using saemix, an r implementation of the saem algorithm. *Journal of Statistical Software*, 2017.
- [11] Frank Dondelinger, Dirk Husmeier, Simon Rogers, and Maurizio Filippone. Ode parameter inference using adaptive gradient matching with gaussian processes. In *Artificial intelligence and statistics*, 2013.
- [12] Shurui Gui, Xiner Li, and Shuiwang Ji. Discovering physics laws of dynamical systems via invariant function learning. In *Proceedings of the 42nd International Conference on Machine Learning*, 2025.
- [13] Oliver Hamelijnc, Arno Solin, and Theodoros Damoulas. Physics-informed variational state-space Gaussian processes. In *Advances in Neural Information Processing Systems*, 2024.
- [14] Pashupati Hegde, Çağatay Yıldız, Harri Lähdesmäki, Samuel Kaski, and Markus Heinonen. Variational multiple shooting for bayesian odes with gaussian processes. In *Uncertainty in Artificial Intelligence*, 2022.
- [15] Markus Heinonen, Cagatay Yildiz, Henrik Mannerstrom, Jukka Intosalmi, and Harri Lahdes-maki. Learning unknown ODE models with gaussian processes. In *Proceedings of the 35th International Conference on Machine Learning*, 2018.
- [16] Patrick Kidger, James Morrill, James Foster, and Terry Lyons. Neural controlled differential equations for irregular time series. *Advances in neural information processing systems*, 2020.
- [17] Matthieu Kirchmeyer, Yuan Yin, Jérémie Donà, Nicolas Baskiotis, Alain Rakotomamonjy, and Patrick Gallinari. Generalizing to new physical systems via context-informed dynamics model. In *International conference on machine learning*, 2022.

- [18] Marc Lavielle. *Mixed Effects Models for the Population Approach: Models, Tasks, Methods and Tools*. CRC press, 2014.
- [19] Arthur Leroy, Pierre Latouche, Benjamin Guedj, and Servane Gey. MAGMA: inference and prediction using multi-task Gaussian processes with common mean. *Machine Learning*, 2022.
- [20] Zhe Li, Mélanie Prague, Rodolphe Thiébaud, and Quentin Clairon. Variational autoencoder for inference of nonlinear mixed effect models based on ordinary differential equations. *arXiv preprint arXiv:2601.17400*, 2026.
- [21] Mary J. Lindstrom and Douglas M. Bates. Nonlinear mixed effects models for repeated measures data. *Biometrics*, 1990.
- [22] Da Long, Zheng Wang, Aditi Krishnapriyan, Robert Kirby, Shandian Zhe, and Michael Mahoney. Autoip: A united framework to integrate physics into gaussian processes. In *International Conference on Machine Learning*, 2022.
- [23] Marco Lorenzi and Maurizio Filippone. Constraining the dynamics of deep probabilistic models. In *Proceedings of the 35th International Conference on Machine Learning*, 2018.
- [24] Daniel Machado, Rafael S Costa, Miguel Rocha, Eugénio C Ferreira, Bruce Tidor, and Isabel Rocha. Modeling formalisms in systems biology. *AMB express*, 2011.
- [25] Julien Martinelli. Position: Biology is the challenge physics-informed ML needs to evolve. In *The Thirty-Ninth Annual Conference on Neural Information Processing Systems Position Paper Track*, 2025.
- [26] S Chandra Mouli, Muhammad Alam, and Bruno Ribeiro. Metaphysica: Improving OOD robustness in physics-informed machine learning. In *The Twelfth International Conference on Learning Representations*, 2024.
- [27] Jurijs Nazarovs, Rudrasis Chakraborty, Songwong Tasneeyapant, Sathya Ravi, and Vikas Singh. A variational approximation for analyzing the dynamics of panel data. In *Proceedings of the Thirty-Seventh Conference on Uncertainty in Artificial Intelligence*, 2021.
- [28] Cesar Ojeda, Niklas Hartung, Wilhelm Huisinga, and Ramses J Sanchez. Amortized in-context mixed effect transformer models: A zero-shot approach for pharmacokinetics. In *The 29th International Conference on Artificial Intelligence and Statistics*, 2026.
- [29] Ali Rahimi and Benjamin Recht. Random features for large-scale kernel machines. In *Advances in Neural Information Processing Systems*, 2007.
- [30] Carl Edward Rasmussen and Christopher K. I. Williams. *Gaussian Processes for Machine Learning*. MIT Press, 2006.
- [31] Yulia Rubanova, Ricky T. Q. Chen, and David Duvenaud. Latent ODEs for irregularly-sampled time series. In *Advances in Neural Information Processing Systems*, 2019.
- [32] Simo Särkkä. *Bayesian Filtering and Smoothing*. Cambridge University Press, 2013.
- [33] Simo Särkkä and Arno Solin. *Applied Stochastic Differential Equations*. Cambridge University Press, 2019.
- [34] Gurjeet Sangra Singh, Frantzeska Lavda, Giangiacomo Mercatali, and Alexandros Kalousis. Variational grey-box dynamics matching. In *Proceedings of The 29th International Conference on Artificial Intelligence and Statistics*, 2026.
- [35] Arno Solin and Simo Särkkä. Hilbert space methods for reduced-rank Gaussian process regression. *Statistics and Computing*, 2020.
- [36] Naoya Takeishi and Alexandros Kalousis. Deep grey-box modeling with adaptive data-driven models toward trustworthy estimation of theory-driven models. In *Proceedings of The 26th International Conference on Artificial Intelligence and Statistics*, 2023.
- [37] Gerald Teschl. *Ordinary differential equations and dynamical systems*. American Mathematical Soc., 2012.
- [38] Filip Tronarp, Hans Kersting, Simo Särkkä, and Philipp Hennig. Probabilistic solutions to ordinary differential equations as nonlinear bayesian filtering: a new perspective. *Statistics and Computing*, 2019.

- [39] Liangliang Wang, Jiguo Cao, James O Ramsay, DM Burger, CJL Laporte, and Jürgen K Rockstroh. Estimating mixed-effects differential equation models. *Statistics and Computing*, 2014.
- [40] Philippe Wenk, Gabriele Abbati, Michael A Osborne, Bernhard Schölkopf, Andreas Krause, and Stefan Bauer. Odin: Ode-informed regression for parameter and state inference in time-continuous dynamical systems. In *Proceedings of the AAAI Conference on Artificial Intelligence*, 2020.
- [41] Shihao Yang, Samuel W. K. Wong, and S. C. Kou. Inference of dynamic systems from noisy and sparse data via manifold-constrained gaussian processes. *Proceedings of the National Academy of Sciences*, 2021.
- [42] Jun Ho Yoon, Daniel P Jeong, and Seyoung Kim. Doubly mixed-effects gaussian process regression. In *International Conference on Artificial Intelligence and Statistics*, 2022.
- [43] Ziang Zhang, Alex Stringer, Patrick Brown, and Jamie Stafford. Model-based smoothing with integrated wiener processes and overlapping splines. *Journal of Computational and Graphical Statistics*, 2024.
- [44] Bob Junyi Zou, Matthew E Levine, Dessi P. Zaharieva, Ramesh Johari, and Emily Fox. Hybrid² neural ODE causal modeling and an application to glycemic response. In *Proceedings of the 41st International Conference on Machine Learning*, 2024.

Appendix

A	Supplementary figures	15
B	Baselines and hyperparameters	18
B.1	Concurrent baselines	18
B.2	Baselines derived from MEGPODE	22
B.3	Hyperparameters	23
C	Additional experimental details	26
C.1	Systems	26
C.2	Lotka–Volterra with subject covariates (2D)	27
C.3	FHN Misspecification Experiment	29
C.4	Hardware	29
D	Additional derivations	29
D.1	Derivation of the local Gaussian pseudo-observation	29
D.2	Trajectory-space Kalman smoothing update	31
D.3	Extrapolation for a trained subject	32
D.4	Adaptation and extrapolation for a new subject after training	33
D.5	Initial conditions	33
D.6	Hyperparameter learning	35
D.7	Field-space updates and conservative shared-field variants	35
D.8	Population trajectory uncertainty via Monte Carlo pushforward	36
D.9	Static subject covariates	36
E	Theoretical properties	36
E.1	Posterior-mean dynamics: well-posedness and trajectory-level deviation bounds	36
E.2	Hierarchical field covariance and predictive uncertainty decompositions	38
E.3	The conditional field update as weighted mixed ridge regression	40
E.4	Spectral shrinkage and effective degrees of freedom	42
E.5	Monotone information accumulation	43
F	Alternative scalable vector field approximations	43

A Supplementary figures

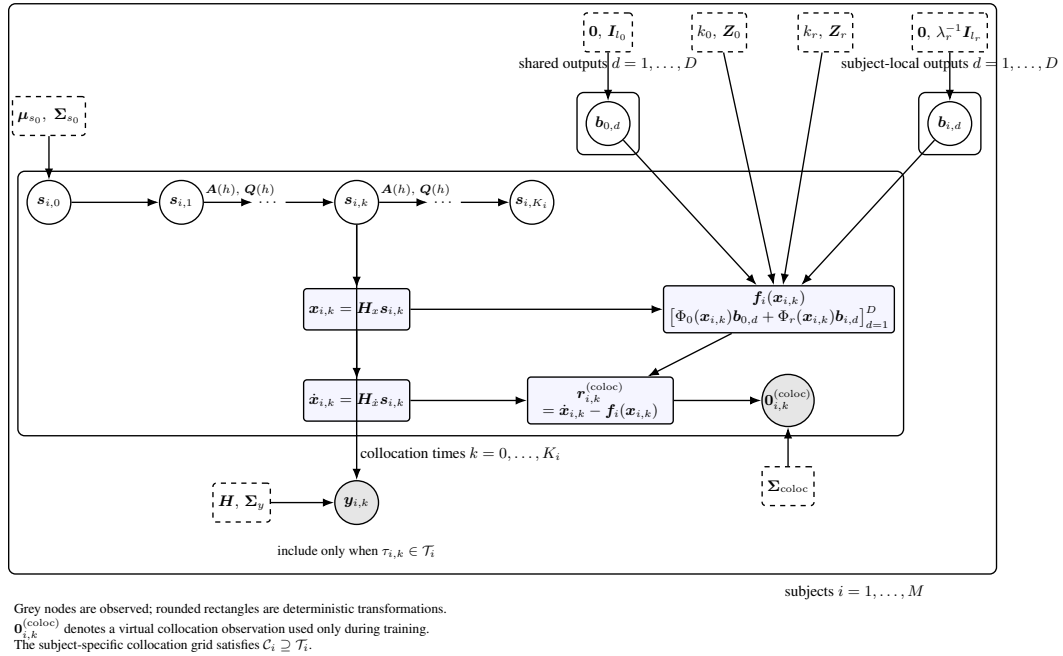


Figure S1: **Full plate diagram of MEGPODEused during training.** The shared vector field is global across subjects, whereas each subject has its own local deviation field. Both act on the latent state extracted from the state-space trajectory prior, and the ODE is enforced through an auxiliary collocation observation.

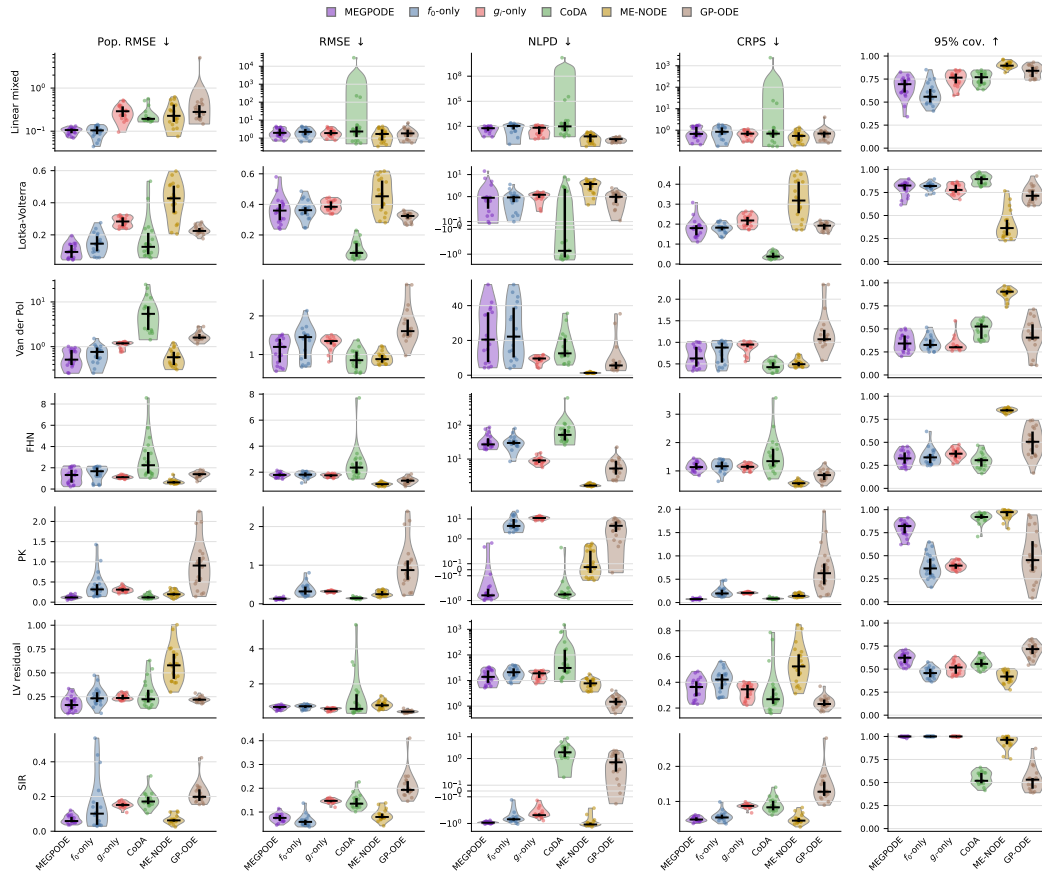


Figure S2: **Forecast performance across synthetic benchmarks.** Distribution of target-window forecast metrics over 20 random seeds for each benchmark system and method. Columns show population RMSE, subject-level RMSE, NLPD, CRPS, and empirical 95% coverage; lower is better except for coverage. Each point is one seed, violins show the seed distribution, and black markers summarize central tendency.

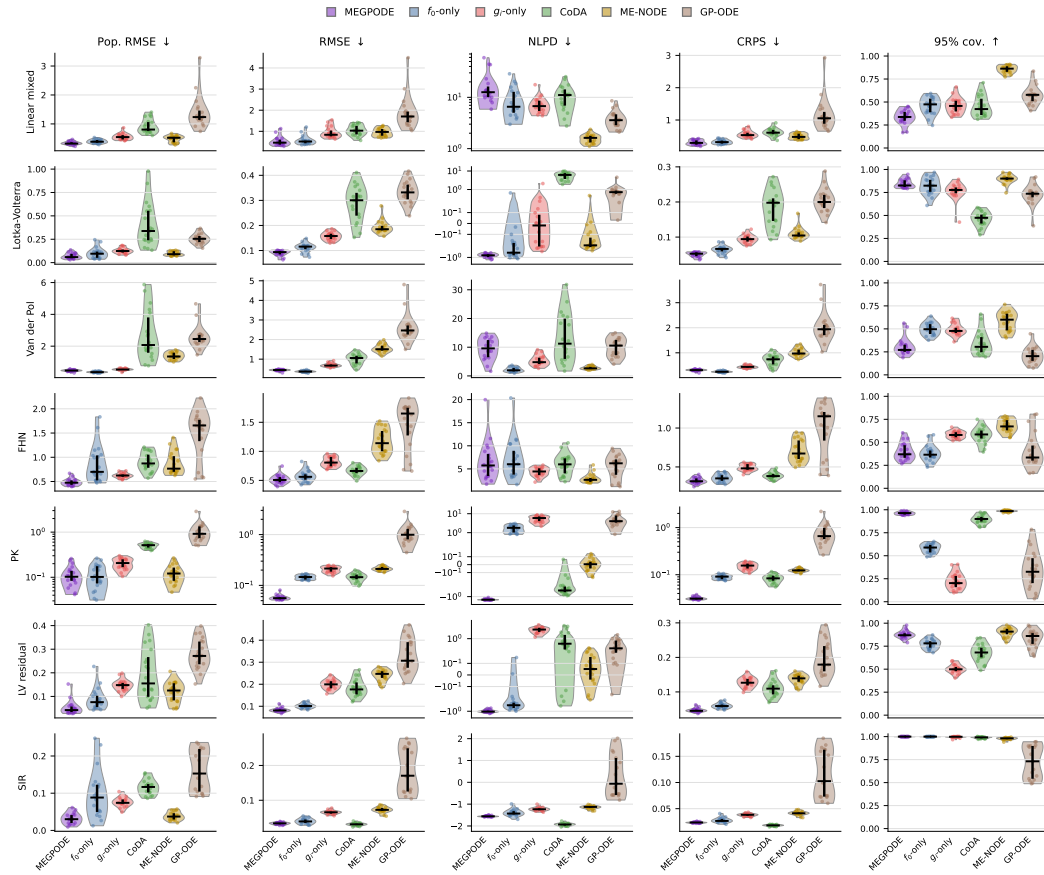


Figure S3: **Interpolation performance across synthetic benchmarks.** Target-window interpolation metrics over 20 random seeds for each benchmark system and method. Columns show population RMSE, subject-level RMSE, NLPD, CRPS, and empirical 95% coverage; lower is better except for coverage. Points are seeds, violins show seed distributions, and black markers summarize central tendency.

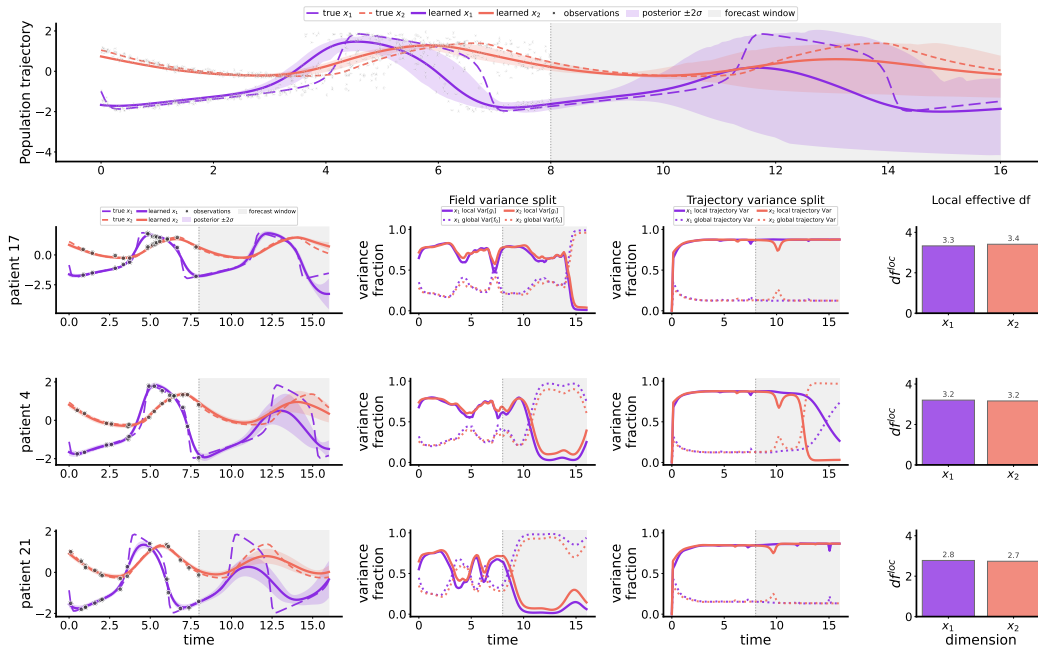


Figure S4: **variance decomposition diagnostics for MEGPODE on the FHN oscillator.** The top panel shows the learned population trajectory with posterior uncertainty and the forecast region. Each lower row shows a representative subject: posterior trajectory reconstruction, decomposition of vector-field uncertainty into population and subject-specific components, the corresponding trajectory-level variance decomposition, and the effective local degrees of freedom by state dimension.

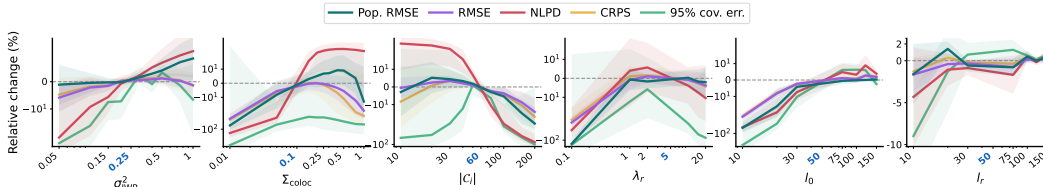


Figure S5: **Ablations on hyperparameters for MEGPODE (interpolation setting).** Each panel varies a single hyperparameter around the default configuration, while keeping the rest of the training and evaluation pipeline fixed; the blue tick marks the default value. Mean ± 0.5 std relative change with respect to the default setting shown, averaged over 10 seeds and the benchmark systems used in the ablation study.

B Baselines and hyperparameters

B.1 Concurrent baselines

CoDA context-conditioned neural ODE. We include a context-conditioned neural ODE baseline inspired by CoDA [17]. In its original setting, different environments share a neural dynamical model but are allowed to induce environment-specific vector fields through learned context variables. We adapt this view to our population setting by treating each training subject as one environment. Each subject has a learned context code $\mathbf{c}_i \in \mathbb{R}^{d_c}$ and a learned initial condition $\mathbf{x}_{i,0}$, and evolves according to

$$\dot{\mathbf{x}}_i(t) = f_{\Theta, \psi}(\mathbf{x}_i(t); \mathbf{c}_i), \quad \mathbf{x}_i(t_{i,0}) = \mathbf{x}_{i,0}.$$

The vector field is represented by a shared base MLP whose weights are additively perturbed by a hypernetwork applied to the context code:

$$f_{\Theta, \psi}(\mathbf{x}; \mathbf{c}) = \text{MLP}_{\Theta + \Delta_\psi(\mathbf{c})}(\mathbf{x}), \quad \Delta_\psi(\mathbf{c}) = A_\psi \mathbf{c}.$$

Thus Θ defines a population neural vector field, while $\Delta_\psi(\mathbf{c}_i)$ defines a subject-specific deformation of that field. Observations are modeled as

$$\mathbf{y}_{i,n} = \mathbf{H}_i \mathbf{x}_i(t_{i,n}) + \varepsilon_{i,n}, \quad \varepsilon_{i,n} \sim \mathcal{N}(0, \sigma_y^2 \mathbf{I}).$$

Training minimizes the pooled reconstruction error over all subjects, jointly over the shared MLP parameters, the hypernetwork, the subject context codes, and the subject initial conditions:

$$\begin{aligned} \min_{\Theta, \psi, \{\mathbf{c}_i, \mathbf{x}_{i,0}\}} & \sum_{i=1}^M \sum_{n=1}^{N_i} \|\mathbf{y}_{i,n} - \mathbf{H}_i \mathbf{x}_i(t_{i,n}; \Theta, \psi, \mathbf{c}_i, \mathbf{x}_{i,0})\|_2^2 \\ & + \lambda_c \sum_i \|\mathbf{c}_i\|_2^2 + \lambda_h \sum_i \|\Delta_\psi(\mathbf{c}_i)\|_2^2 + \lambda_x \sum_i \|\mathbf{x}_{i,0} - \bar{\mathbf{x}}_0\|_2^2. \end{aligned}$$

Here $\bar{\mathbf{x}}_0$ denotes the empirical center of the learned subject initial conditions. In our implementation, trajectories are integrated with a fixed-step RK4 solver, and σ_y is set from the final training RMSE with a small floor.

For held-out-subject adaptation, the shared network and hypernetwork are frozen. Only a new context code and initial condition are optimized from the available context observations:

$$(\hat{\mathbf{c}}_*, \hat{\mathbf{x}}_{*,0}) = \arg \min_{\mathbf{c}, \mathbf{x}_0} \sum_{n \in \mathcal{C}_*} \|\mathbf{y}_{*,n} - \mathbf{H}_* \mathbf{x}_*(t_{*,n}; \Theta, \psi, \mathbf{c}, \mathbf{x}_0)\|_2^2 + \lambda_c \|\mathbf{c}\|_2^2 + \lambda_x \|\mathbf{x}_0 - \bar{\mathbf{x}}_0\|_2^2.$$

Hence CoDA can personalize dynamics through a low-dimensional context variable, but it does not explicitly decompose the field into a shared GP component plus a subject-specific random-effect field. For population-level summaries, we therefore define the CoDA population field as the empirical average of the learned subject-specific context fields,

$$f_{\text{CoDA}}^{\text{POP}}(\mathbf{x}) = \frac{1}{M} \sum_{i=1}^M f_{\Theta, \psi}(\mathbf{x}; \mathbf{c}_i).$$

Since the mapping from context code to vector field acts through weight perturbations, averaging the resulting vector fields is more faithful than evaluating the model at the empirical mean context code.

The population trajectory is obtained by integrating this averaged field from the empirical mean initial condition,

$$\dot{\mathbf{x}}^{\text{POP}}(t) = f_{\text{CoDA}}^{\text{POP}}(\mathbf{x}^{\text{POP}}(t)), \quad \mathbf{x}^{\text{POP}}(0) = \bar{\mathbf{x}}_0 = \frac{1}{M} \sum_{i=1}^M \mathbf{x}_{i,0}.$$

The baseline is therefore deterministic apart from the scalar Gaussian observation noise used for predictive scores; it does not maintain a posterior over vector fields.

Mixed-effect neural ODE. We further include a mixed-effect neural ODE baseline based on [27]. This model represents each subject through a latent trajectory $\mathbf{z}_i(t) \in \mathbb{R}^{d_z}$, decoded into observation space by a neural decoder D_ω :

$$\mathbf{y}_{i,n} = D_\omega(\mathbf{z}_i(t_{i,n})) + \varepsilon_{i,n}, \quad \varepsilon_{i,n} \sim \mathcal{N}(0, \sigma_y^2 \mathbf{I}).$$

The initial latent state is inferred amortizedly from the subject’s observed time series using an encoder,

$$q_\phi(\mathbf{z}_{i,0} \mid \{(t_{i,n}, \mathbf{y}_{i,n})\}_{n \in \mathcal{C}_i}),$$

implemented either as an ODE-RNN or an RNN encoder. Subject heterogeneity enters the latent vector field through mixed-effect weights. Concretely, the latent drift is written as

$$\dot{\mathbf{z}}_i(t) = G_\theta(\mathbf{z}_i(t)) \mathbf{w}_i,$$

where G_θ is a shared neural network and the subject-specific mixed-effect weights are sampled from a diagonal Gaussian distribution

$$\mathbf{w}_i = \boldsymbol{\mu}_w + \boldsymbol{\sigma}_w \odot \boldsymbol{\epsilon}_i, \quad \boldsymbol{\epsilon}_i \sim \mathcal{N}(\mathbf{0}, \mathbf{I}).$$

Thus the model has a neural population component through G_θ and $\boldsymbol{\mu}_w$, together with random effects through $\boldsymbol{\sigma}_w$.

The training objective is a variational reconstruction objective with KL terms for both the inferred initial state and the mixed-effect weights. In simplified form,

$$\begin{aligned} \mathcal{L}_{\text{ME-NODE}} = & \sum_{i=1}^M \mathbb{E}_{q_\phi(\mathbf{z}_{i,0}|\mathbf{y}_i) q(\mathbf{w}_i)} [\log p(\mathbf{y}_i | \mathbf{z}_{i,0}, \mathbf{w}_i, \theta, \omega)] \\ & - \beta_z \text{KL}(q_\phi(\mathbf{z}_{i,0} | \mathbf{y}_i) \| p(\mathbf{z}_0)) - \beta_w \text{KL}(q(\mathbf{w}_i) \| p(\mathbf{w})), \end{aligned}$$

with KL annealing during training. In the implementation used here, several samples of $\mathbf{z}_{i,0}$ and \mathbf{w}_i are drawn, and the best reconstruction among these samples is used for the subject loss. Training proceeds one subject at a time so that irregular subject-specific observation grids are preserved.

For held-out subjects, there is no separate optimization of new parameters. Instead, the learned encoder and mixed-effect distribution are reused: the context observations of the new subject are passed through the encoder, candidate mixed-effect samples are drawn, and the context-compatible samples determine the predictive distribution. Thus adaptation is amortized rather than obtained by a subject-specific optimization loop.

At evaluation time, for each subject i , we draw candidate samples

$$\mathbf{z}_{i,0}^{(s)} \sim q_\phi(\mathbf{z}_{i,0} | \mathbf{y}_i), \quad \mathbf{w}_i^{(s)} \sim q(\mathbf{w}_i), \quad s = 1, \dots, S_{\text{cand}},$$

rank them by reconstruction error on the available context observations, and retain S context-compatible samples. Each retained sample is propagated through the latent ODE,

$$\dot{\mathbf{z}}_i^{(s)}(t) = G_\theta(\mathbf{z}_i^{(s)}(t))\mathbf{w}_i^{(s)}, \quad \hat{\mathbf{x}}_i^{(s)}(t) = D_\omega(\mathbf{z}_i^{(s)}(t)).$$

The reported posterior predictive mean and epistemic standard deviation are then

$$\hat{\boldsymbol{\mu}}_i(t) = \frac{1}{S} \sum_{s=1}^S \hat{\mathbf{x}}_i^{(s)}(t), \quad \hat{\boldsymbol{\sigma}}_{i,\text{post}}^2(t) = \frac{1}{S} \sum_{s=1}^S \left(\hat{\mathbf{x}}_i^{(s)}(t) - \hat{\boldsymbol{\mu}}_i(t) \right)^2.$$

For probabilistic trajectory scores and predictive bands, we add the learned scalar observation noise,

$$\hat{\boldsymbol{\sigma}}_{i,\text{pred}}^2(t) = \hat{\boldsymbol{\sigma}}_{i,\text{post}}^2(t) + \hat{\boldsymbol{\sigma}}_y^2.$$

For population-level summaries, this baseline does not expose an explicit vector field in the original observation space. We therefore define its population trajectory operationally by averaging sampled subject trajectories over a fixed subset \mathcal{I} of training subjects:

$$\hat{\mathbf{x}}_{\text{ME-NODE}}^{\text{pop},(s)}(t) = \frac{1}{|\mathcal{I}|} \sum_{i \in \mathcal{I}} D_\omega(\mathbf{z}_i^{(s)}(t)).$$

The reported population mean and posterior uncertainty are computed across these Monte Carlo population trajectories. This gives ME-NODE subject-level and population-level uncertainty over latent initial states and mixed-effect weights, but not a posterior over the shared neural vector field parameters θ , which remain point estimates.

GPODE variational multiple shooting with shared field and subject-specific initial conditions.

As a non-mixed-effect GP-ODE comparator, we adapt the variational multiple-shooting model of Hegde et al. [14] to the population setting by forcing all subjects to share a single latent vector field, while allowing each subject to have its own initial condition and its own auxiliary shooting states. Concretely, we fit

$$\dot{\mathbf{x}}_i(t) = \mathbf{f}(\mathbf{x}_i(t)), \quad \mathbf{x}_i(t_{i,0}) = \mathbf{x}_{i,0}, \quad i = 1, \dots, M,$$

under one common GP prior and one shared variational posterior for \mathbf{f} , with subject-specific variational factors for $\mathbf{x}_{i,0}$ and for the shooting states. Hence this baseline can exploit multiple initial conditions and long trajectories, but it has no explicit mixed-effect decomposition: all inter-subject variation must be absorbed through the subject-specific initial conditions, the subject-specific shooting states, and posterior uncertainty in the single shared field.

In addition to the subject-specific initial conditions $\mathbf{x}_{i,0}$, auxiliary shooting states are introduced

$$\mathbf{S}_i := (\mathbf{s}_{i,1}, \dots, \mathbf{s}_{i,N_i-1}), \quad \mathbf{s}_{i,0} := \mathbf{x}_{i,0}, \quad i = 1, \dots, M.$$

All subjects share the same latent vector field \mathbf{f} and the same inducing variables \mathbf{U} . The shooting transition is

$$p(\mathbf{s}_{i,n} | \mathbf{s}_{i,n-1}, \mathbf{f}) = \mathcal{N}(\mathbf{s}_{i,n} | \mathbf{x}(t_{i,n}; \mathbf{s}_{i,n-1}, \mathbf{f}), \sigma_{\xi}^2 \mathbf{I}_D), \quad n = 1, \dots, N_i - 1,$$

where $\mathbf{x}(t_{i,n}; \mathbf{s}_{i,n-1}, \mathbf{f})$ denotes the ODE solution at time $t_{i,n}$ obtained by integrating $\dot{\mathbf{x}}(t) = \mathbf{f}(\mathbf{x}(t))$ from initial state $\mathbf{s}_{i,n-1}$ over $[t_{i,n-1}, t_{i,n}]$. The observation likelihood is written similarly as

$$p(\mathbf{y}_{i,n} | \mathbf{s}_{i,n-1}, \mathbf{f}) = p(\mathbf{y}_{i,n} | \mathbf{x}(t_{i,n}; \mathbf{s}_{i,n-1}, \mathbf{f})).$$

A natural variational family is

$$q(\{\mathbf{S}_i\}_{i=1}^M, \{\mathbf{x}_{i,0}\}_{i=1}^M, \mathbf{f}, \mathbf{U}) = p(\mathbf{f} | \mathbf{U}) q(\mathbf{U}) \prod_{i=1}^M \left[q(\mathbf{x}_{i,0}) \prod_{n=1}^{N_i-1} q(\mathbf{s}_{i,n}) \right].$$

The resulting population ELBO is

$$\begin{aligned} \mathcal{L}_{\text{GPODE-pop}} = & \sum_{i=1}^M \left[\sum_{n=1}^{N_i} \mathbb{E}_{q(\mathbf{s}_{i,n-1}) q(\mathbf{f})} \left[\log p(\mathbf{y}_{i,n} | \mathbf{s}_{i,n-1}, \mathbf{f}) \right] \right. \\ & + \sum_{n=1}^{N_i-1} \mathbb{E}_{q(\mathbf{s}_{i,n-1}) q(\mathbf{s}_{i,n}) q(\mathbf{f})} \left[\log p(\mathbf{s}_{i,n} | \mathbf{s}_{i,n-1}, \mathbf{f}) \right] \\ & \left. - \sum_{n=1}^{N_i-1} \mathbb{E}_{q(\mathbf{s}_{i,n})} \left[\log q(\mathbf{s}_{i,n}) \right] - \text{KL}(q(\mathbf{x}_{i,0}) \| p(\mathbf{x}_{i,0})) \right] - \text{KL}(q(\mathbf{U}) \| p(\mathbf{U})). \end{aligned}$$

The training objective sums the subject-wise likelihood and shooting terms under this common field, together with a single shared inducing-variable KL term.

For comparability with our population-level summaries, we define the corresponding population trajectory by integrating the posterior-mean shared field

$$\bar{\mathbf{f}}(\mathbf{x}) := \mathbb{E}_q[\mathbf{f}(\mathbf{x})]$$

from a reference initial condition $\mathbf{x}_0^{\text{pop}}$, for example the empirical mean of the subject-specific initial conditions:

$$\dot{\mathbf{x}}^{\text{pop}}(t) = \bar{\mathbf{f}}(\mathbf{x}^{\text{pop}}(t)), \quad \mathbf{x}^{\text{pop}}(0) = \mathbf{x}_0^{\text{pop}}.$$

Uncertainty for this population trajectory can be approximated by Monte Carlo pushforward of samples from the learned field posterior, all propagated from the same reference initial condition.

Mechanistic NLME-ODE. For benchmarks whose mechanistic family is known, we include a classical nonlinear mixed-effects ODE baseline [10, 18]. We assume that each subject follows a parametric ODE

$$\dot{\mathbf{x}}_i(t) = f(\mathbf{x}_i(t); \boldsymbol{\theta}_i), \quad \boldsymbol{\theta}_i = \boldsymbol{\theta} + \boldsymbol{\eta}_i, \quad \boldsymbol{\eta}_i \sim \mathcal{N}(\mathbf{0}, \boldsymbol{\Omega}),$$

with subject-specific initial condition

$$\mathbf{x}_i(t_{i,0}) = \mathbf{x}_{i,0}, \quad \mathbf{x}_{i,0} = \mathbf{x}_0 + \boldsymbol{\xi}_i, \quad \boldsymbol{\xi}_i \sim \mathcal{N}(\mathbf{0}, \boldsymbol{\Omega}_{x_0}), \quad i = 1, \dots, M,$$

where $\boldsymbol{\theta}$ collects shared population parameters, $\boldsymbol{\eta}_i$ denotes subject-specific random effects on the mechanistic parameters, and \mathbf{x}_0 is the population initial condition. In practice, random effects act only on a subset of mechanistic parameters, with the remaining components fixed across subjects. Observations are modeled as

$$\mathbf{y}_{i,n} = \mathbf{H}_i \mathbf{x}_i(t_{i,n}) + \boldsymbol{\varepsilon}_{i,n}, \quad \boldsymbol{\varepsilon}_{i,n} \sim \mathcal{N}(0, \sigma_y^2 \mathbf{I}).$$

On correctly specified mechanistic systems, the random effects are placed on the same parameters used to generate heterogeneity in the benchmark.

We fit this model with a SAEM-style empirical-Bayes procedure. At iteration m , we first compute, for each subject i , a conditional mode

$$\begin{aligned} (\hat{\boldsymbol{\eta}}_i^{(m)}, \hat{\boldsymbol{\xi}}_i^{(m)}) = \arg \min_{\boldsymbol{\eta}_i, \boldsymbol{\xi}_i} & \left[\frac{1}{2 \left(\sigma_y^{(m-1)} \right)^2} \sum_n \left\| \mathbf{y}_{i,n} - \mathbf{H}_i \mathbf{x}_i(t_{i,n}; \boldsymbol{\theta}^{(m-1)}, \boldsymbol{\eta}_i, \mathbf{x}_0^{(m-1)} + \boldsymbol{\xi}_i) \right\|_2^2 \right. \\ & \left. + \frac{1}{2} \boldsymbol{\eta}_i^\top \boldsymbol{\Omega}^{(m-1)-1} \boldsymbol{\eta}_i + \frac{1}{2} \boldsymbol{\xi}_i^\top \boldsymbol{\Omega}_{x_0}^{(m-1)-1} \boldsymbol{\xi}_i \right], \end{aligned}$$

where $\mathbf{x}_i(t; \boldsymbol{\theta}, \boldsymbol{\eta}_i, \mathbf{x}_{i,0})$ is obtained by numerical integration of the mechanistic ODE. Given the current subject modes, we then perform a single population M-step:

$$\begin{aligned} \boldsymbol{\theta}^{(m)} &= \arg \min_{\boldsymbol{\theta}} \sum_{i,n} \left\| \mathbf{y}_{i,n} - \mathbf{H}_i \mathbf{x}_i(t_{i,n}; \boldsymbol{\theta}, \hat{\boldsymbol{\eta}}_i^{(m)}, \mathbf{x}_0^{(m-1)} + \hat{\boldsymbol{\xi}}_i^{(m)}) \right\|_2^2, \\ \mathbf{x}_0^{(m)} &= \frac{1}{M} \sum_{i=1}^M \hat{\mathbf{x}}_{i,0}^{(m)} = \mathbf{x}_0^{(m-1)} + \frac{1}{M} \sum_{i=1}^M \hat{\boldsymbol{\xi}}_i^{(m)}, \\ \boldsymbol{\Omega}^{(m)} &= \text{Diag} \left(\frac{1}{M} \sum_{i=1}^M \left(\hat{\boldsymbol{\eta}}_i^{(m)} \right)^2 \right), \\ \boldsymbol{\Omega}_{x_0}^{(m)} &= \text{Diag} \left(\frac{1}{M} \sum_{i=1}^M \left(\hat{\boldsymbol{\xi}}_i^{(m)} \right)^2 \right), \\ \sigma_y^{2(m)} &= \frac{1}{N_{\text{obs}}} \sum_{i,n} \left\| \mathbf{y}_{i,n} - \mathbf{H}_i \mathbf{x}_i(t_{i,n}; \boldsymbol{\theta}^{(m)}, \hat{\boldsymbol{\eta}}_i^{(m)}, \mathbf{x}_0^{(m)} + \hat{\boldsymbol{\xi}}_i^{(m)}) \right\|_2^2. \end{aligned}$$

These two steps are repeated for a fixed number of iterations. For held-out-subject adaptation, the learned population parameters are kept fixed and only the new subject's random effects and initial condition are re-estimated from the available context observations.

This baseline provides a standard parametric NLME comparator when the mechanistic family is known, but it is structurally misspecified on benchmarks where heterogeneity is injected through residual subject-specific vector fields rather than through parameter random effects.

For comparability with our population-level summaries, we define the corresponding population trajectory by integrating the learned mechanistic population dynamics from the learned population initial condition:

$$\dot{\mathbf{x}}^{\text{pop}}(t) = f\left(\mathbf{x}^{\text{pop}}(t); \hat{\boldsymbol{\theta}}\right), \quad \mathbf{x}^{\text{pop}}(0) = \hat{\mathbf{x}}_0.$$

B.2 Baselines derived from MEGPODE

We compare the full mixed-effect model against two controlled ablations that keep the same trajectory prior, the same collocation construction in Eqs. (19)–(20), and the same pseudo-derivative extraction in Eq. (21). The only difference is which components of the subject-specific field are allowed to explain the dynamics.

Shared field only ($\mathbf{f0_only}$). This ablation removes the subject-specific deviation altogether and forces all subjects to share a single population field:

$$f_{i,d}^{\mathbf{f0_only}}(\mathbf{x}) = f_{0,d}(\mathbf{x}) \approx \Phi_0(\mathbf{x}) \mathbf{b}_{0,d}, \quad g_{i,d}(\mathbf{x}) \equiv 0.$$

The pseudo-regression of Eq. (24) therefore reduces to

$$\mathbf{u}_{i,d} = \mathbf{P}_{0,i,d} \mathbf{b}_{0,d} + \boldsymbol{\varepsilon}_{i,d}^{\text{reg}} \quad \boldsymbol{\varepsilon}_{i,d}^{\text{reg}} \sim \mathcal{N}(\mathbf{0}, \mathbf{R}_{i,d}),$$

so only the shared posterior is updated:

$$\begin{aligned} \boldsymbol{\Lambda}_{0,d}^{\text{new}} &= \mathbf{I}_{l_0} + \sum_{i=1}^M \mathbf{P}_{0,i,d}^\top \mathbf{R}_{i,d}^{-1} \mathbf{P}_{0,i,d}, \\ \boldsymbol{\eta}_{0,d}^{\text{new}} &= \sum_{i=1}^M \mathbf{P}_{0,i,d}^\top \mathbf{R}_{i,d}^{-1} \mathbf{u}_{i,d}. \end{aligned}$$

There is no local-field update. In trajectory space, the collocation moments $(\mu_{i,k}^f, \Sigma_{i,k}^f, \mathbf{J}_{i,k})$ are therefore computed from the shared field alone. This baseline isolates how much of the data can be explained by a single population ODE with no subject-specific adaptation.

One field per subject, no shared component (`gi_only`). This ablation removes the common field and learns one independent field for each subject:

$$f_{i,d}^{\text{gi_only}}(\mathbf{x}) = g_{i,d}(\mathbf{x}) \approx \Phi_r(\mathbf{x})\mathbf{b}_{i,d}, \quad f_{0,d}(\mathbf{x}) \equiv 0.$$

The priors are

$$\mathbf{b}_{i,d} \sim \mathcal{N}(\mathbf{0}, \lambda_r^{-1} \mathbf{I}_{l_r}), \quad i = 1, \dots, M.$$

The pseudo-regression now factorizes over subjects:

$$\mathbf{u}_{i,d} = \mathbf{P}_{r,i,d} \mathbf{b}_{i,d} + \boldsymbol{\varepsilon}_{i,d}^{\text{reg}} \quad \boldsymbol{\varepsilon}_{i,d}^{\text{reg}} \sim \mathcal{N}(\mathbf{0}, \mathbf{R}_{i,d}),$$

and each local posterior is updated independently:

$$\begin{aligned} \boldsymbol{\Lambda}_{i,d}^{\text{new}} &= \lambda_r \mathbf{I}_{l_r} + \mathbf{P}_{r,i,d}^\top \mathbf{R}_{i,d}^{-1} \mathbf{P}_{r,i,d}, \\ \boldsymbol{\eta}_{i,d}^{\text{new}} &= \mathbf{P}_{r,i,d}^\top \mathbf{R}_{i,d}^{-1} \mathbf{u}_{i,d}. \end{aligned}$$

Hence there is no cross-subject borrowing through a shared latent field. This baseline isolates the value of explicitly modeling a population-level dynamical component.

Relation to the full model. The full method combines both ingredients,

$$f_{i,d}(\mathbf{x}) = \Phi_0(\mathbf{x})\mathbf{b}_{0,d} + \Phi_r(\mathbf{x})\mathbf{b}_{i,d},$$

and updates the shared and local posteriors by alternating the regressions in Eqs. (25)–(28). Thus `f0_only` tests whether a single shared ODE is sufficient, while `indep_fields` tests whether sharing is necessary at all. At deployment time this distinction is also important: `f0_only` yields a population forecast but no personalization, whereas `indep_fields` can only personalize from the new subject’s own data.

B.3 Hyperparameters

Table S1: Hyperparameter settings for CODA, GP-ODE, and ME-NODE

Hyperparameter	Value
CODA	
State dimension	benchmark latent dimension D
Base MLP widths	$D \rightarrow 64 \rightarrow 64 \rightarrow 64 \rightarrow D$
Hidden dimension	64
Hidden activation	SiLU(x)/1.1
Output scale factor	1.0
Context code dimension	2
Context codes	one learned code per training patient
Hypernetwork	linear map from context code to additive offsets for all base MLP weights and biases
Base weight initialization	Xavier uniform
Base bias initialization	zeros
Final layer initialization	final weight matrix multiplied by 0.1
Optimizer	Adam
Learning rate	10^{-3}
Max training epochs	10000
Initial-condition initialization	first observed value per subject and dimension
Context-code regularization	10^{-4}
Hypernetwork-offset regularization	10^{-6}

Hyperparameter	Value
Initial-condition regularization	10^{-3}
ODE solver	fixed-step RK4
RK4 substeps per interval	1
Held-out adaptation variables	new context code and new initial condition
Held-out adaptation epochs	2000
Held-out adaptation learning rate	same as training learning rate, 10^{-3}
Population field	average of context-conditioned fields over training context codes
GP-ODE	
Kernel	RBF
Kernel parameterization	output-dimension-wise lengthscales and variances
Initial RBF lengthscale	1.3
Initial RBF variance	0.5
Number of inducing points	16
Inducing initialization	k -means centers on training states
Inducing value initialization	empirical finite-difference gradients
Random Fourier features	256
Inducing posterior covariance	full covariance
Likelihood	Gaussian
Likelihood variance	learned by default
State posterior	factorized Gaussian shooting-state variational posterior
State-continuity constraint	Gaussian
Constraint initial scale	10^{-3}
Constraint trainable	false
Optimizer	Adam
Learning rate	5×10^{-3}
Training iterations	10000
Monte Carlo samples in objective	5
ODE solver	dopri5 via torchdiffeq
Dense-time scale	4
Evaluation samples	16
Held-out adaptation variables	initial condition only
Held-out adaptation epochs	300
Held-out adaptation learning rate	same as training learning rate, 5×10^{-3}
Held-out initial-condition penalty	10^{-3} toward population initial condition
Prediction std.	posterior sample std. plus likelihood noise
ME-NODE	
Latent dimension	13
Recognition dimension	20
Recognition layers	1
GRU units	100
Initial-state encoder	ODE-RNN
Encoder input	observations concatenated with observation masks
Encoder ODE solver	Euler
Encoder ODE tolerances	rtol 10^{-3} , atol 10^{-4}
Generative ODE network layers	1
Generative ODE hidden units	100
Generative ODE activation	Tanh
Generative ODE widths	13 \rightarrow 100 \rightarrow 100 \rightarrow 13
Mixed-effect dimension	1
Mixed-effect layer	learned fixed effect plus diagonal random-effect std.
Decoder	linear map 13 \rightarrow D
Initial-state prior	standard normal

Hyperparameter	Value
Observation std. in training likelihood	0.1
Optimizer	Adamax
Learning rate	10^{-3}
Learning-rate scheduler	exponential decay
Scheduler decay	$\gamma = 0.999$
Training epochs	1000
Gradient clipping	global norm 1.0
KL annealing epochs	100
KL annealing start epoch	1
Initial-state samples n_{z_0}	1
Mixed-effect samples n_w	20
Evaluation samples	10
Generative ODE solver	RK4
Generative ODE tolerances	rtol 10^{-3} , atol 10^{-4}
Held-out adaptation	none; prediction conditions through encoder context
Predictive std.	posterior sample std. plus $\max(10^{-3}, \text{train RMSE})$ noise estimate

Table S2: Hyperparameter settings for MEGPODE

Hyperparameter	Value
MEGPODE model	
State smoother	second-order integrated Wiener process prior over $(\mathbf{x}, \dot{\mathbf{x}})$
Field decomposition	$\mathbf{f}_i(\mathbf{x}) = \mathbf{f}_0(\mathbf{x}) + \mathbf{g}_i(\mathbf{x})$
Population field	whitened RBF/Nyström feature field \mathbf{f}_0
Subject-specific field	whitened RBF/Nyström residual field \mathbf{g}_i
Residual prior	$\mathbf{w}_{i,d} \sim \mathcal{N}(\mathbf{0}, \lambda_r^{-1} \mathbf{I})$ independently across subjects and state dimensions
Kernel	ARD RBF kernel for both population and residual fields
Inducing points	$l_0 = l_r = 50$ selected from pooled observed states
Initial RBF lengthscales	0.8 \mathbf{f}_0 , 1.0 for \mathbf{g}_i
Initial kernel variances	1.0 for \mathbf{f}_0 , 0.2 for \mathbf{g}_i
Residual precision	$\lambda_r = 5.0$
Training	
Collocation grid \mathcal{C}_i	observation times merged with 60 uniform points per subject
Observation noise initialization	dataset scale
Collocation covariance	$\Sigma_{\text{coloc}} = \sigma_c^2 \mathbf{I}$, with $\sigma_c = 0.1$ by default
Training iterations	30
Smoother iterations per fit	8 outer linearization iterations
Field update inner iterations	2
Common-field update	collapsed Gaussian update
Hyperparameter learning	
Start time	after 25% of training iterations
Optimization budget	8 optimizer iterations per hyperparameter update
Learned quantities	RBF lengthscales, output scales, σ_y , λ_r , and q_{process}
Parametric and held-out variants	
Held-out adaptation variables	new subject residual field and initial condition; learned population field fixed
Held-out prefix	first 40% of observations
Held-out adaptation iterations	10 iterations

Hyperparameter	Value
Held-out residual precision	$\lambda_{r,\text{adapt}} = 2.5$
Population prediction	Monte Carlo propagation from the learned population initial-condition distribution
Population MC samples	500 by default

C Additional experimental details

C.1 Systems

We now list the benchmark systems used during the experiments of (Section 5.1). All synthetic benchmarks are autonomous first-order ODEs with full-state observations

$$\mathbf{y}_{i,n} = \mathbf{x}_i(t_{i,n}) + \boldsymbol{\epsilon}_{i,n}, \quad \boldsymbol{\epsilon}_{i,n} \sim \mathcal{N}(\mathbf{0}, \sigma_y^2 \mathbf{I}_D),$$

where the observation times are irregular and obtained by sorting i.i.d. draws from $\mathcal{U}([0, T])$. Dense ground-truth trajectories are generated numerically on a fine grid. In the experiments reported, unless stated otherwise in a dedicated ablation, we use the same simulation budget across systems:

$$M = 30, \quad N_{\text{obs}} = 20, \quad \sigma_y = 0.05.$$

Each subject has its own randomized initial condition and the full latent state is observed with additive Gaussian noise, except, again, in a dedicated ablation. Figure S6 displays, for one representative seed, the population and patient trajectories together with the observation horizon, forecasting horizon, and interpolation window for all synthetic systems.

Linear oscillator (2D). For $\mathbf{x}_i = (x_{1,i}, x_{2,i})^\top$,

$$\begin{aligned} \dot{x}_{1,i} &= -\alpha_i x_{1,i} + \beta_i x_{2,i}, \\ \dot{x}_{2,i} &= -\kappa_i x_{1,i} - \gamma_i x_{2,i}. \end{aligned}$$

The population field uses $(\alpha_0, \beta_0, \kappa_0, \gamma_0)$, while subject heterogeneity is introduced through

$$\alpha_i = \alpha_0 + \alpha_{\text{sd}} \xi_i, \quad \beta_i = \beta_0 + \beta_{\text{sd}} \zeta_i, \quad \kappa_i = \kappa_0 + \kappa_{\text{sd}} \rho_i, \quad \gamma_i = \gamma_0 + \gamma_{\text{sd}} \eta_i,$$

with

$$\xi_i, \zeta_i, \rho_i, \eta_i \sim \mathcal{N}(0, 1)$$

independently.

Lotka–Volterra (2D). For prey $x_{1,i}$ and predator $x_{2,i}$,

$$\begin{aligned} \dot{x}_{1,i} &= \alpha_0 x_{1,i} - \beta_i x_{1,i} x_{2,i}, \\ \dot{x}_{2,i} &= \delta_i x_{1,i} x_{2,i} - \gamma_0 x_{2,i}. \end{aligned}$$

The subject-specific random effects act on the interaction coefficients,

$$\beta_i = \beta_0 \exp(\beta_{\text{sd}} \xi_i), \quad \delta_i = \delta_0 \exp(\delta_{\text{sd}} \zeta_i), \quad \xi_i, \zeta_i \sim \mathcal{N}(0, 1).$$

Thus the population field is determined by $(\alpha_0, \beta_0, \delta_0, \gamma_0)$, while subject heterogeneity enters through (β_i, δ_i) .

Van der Pol (2D). For $\mathbf{x}_i = (x_{1,i}, x_{2,i})^\top$,

$$\begin{aligned} \dot{x}_{1,i} &= x_{2,i}, \\ \dot{x}_{2,i} &= \mu_i (1 - x_{1,i}^2) x_{2,i} - x_{1,i}. \end{aligned}$$

Subject variability is introduced through

$$\mu_i = \mu_0 (1 + \mu_{\text{sd}} \xi_i), \quad \xi_i \sim \mathcal{N}(0, 1).$$

FitzHugh–Nagumo (2D). For membrane potential v_i and recovery variable w_i ,

$$\begin{aligned}\dot{v}_i &= s_0 \left(v_i - \frac{v_i^3}{3} - c_i w_i + I_0 \right), \\ \dot{w}_i &= s_0 \frac{d_i v_i + a_0 - b_0 w_i}{\tau_0}.\end{aligned}$$

The subject-specific random effects act on the coupling coefficients,

$$c_i = c_0 + c_{\text{sd}} \xi_i, \quad d_i = d_0 + d_{\text{sd}} \zeta_i, \quad \xi_i, \zeta_i \sim \mathcal{N}(0, 1).$$

One-compartment pharmacokinetics (2D). With gastrointestinal amount $A_{\text{GI},i}$ and plasma concentration $U_{P,i}$,

$$\begin{aligned}\dot{A}_{\text{GI},i} &= -k_{a,i} A_{\text{GI},i}, \\ \dot{U}_{P,i} &= \frac{k_{a,i}}{V_i} A_{\text{GI},i} - k_{e,i} U_{P,i}.\end{aligned}$$

Here heterogeneity is parametric and log-normal:

$\log k_{a,i} = \log k_{a,0} + \sigma_{k_a} \xi_i$, $\log k_{e,i} = \log k_{e,0} + \sigma_{k_e} \zeta_i$, $\log V_i = \log V_0 + \sigma_V \rho_i$, with $\xi_i, \zeta_i, \rho_i \sim \mathcal{N}(0, 1)$. The initial condition is fixed to a common oral dose, $A_{\text{GI},i}(0) = \text{dose}_0$ and $U_{P,i}(0) = 0$.

SIR (3D). For susceptible, infectious, and removed states (S_i, I_i, R_i) ,

$$\begin{aligned}\dot{S}_i &= -\beta_i \frac{S_i I_i}{N_i}, \\ \dot{I}_i &= \beta_i \frac{S_i I_i}{N_i} - \gamma_i I_i, \\ \dot{R}_i &= \gamma_i I_i,\end{aligned}$$

where $N_i = S_i + I_i + R_i$. The subject-specific effects are log-normal:

$$\beta_i = \beta_0 \exp(\sigma_\beta \xi_i), \quad \gamma_i = \gamma_0 \exp(\sigma_\gamma \zeta_i), \quad \xi_i, \zeta_i \sim \mathcal{N}(0, 1).$$

Lotka–Volterra with GP-draw random effects (2D). This benchmark keeps the population dynamics exactly Lotka–Volterra, but replaces parametric subject heterogeneity by smooth subject-specific residual vector fields:

$$\dot{\mathbf{x}}_i(t) = \mathbf{f}_{\text{LV}}(\mathbf{x}_i(t); \theta_0) + \mathbf{g}_i(\mathbf{x}_i(t)), \quad \theta_0 = (\alpha_0, \beta_0, \delta_0, \gamma_0).$$

Each residual component is generated based on a bounded RBF/Nyström GP draw

$$g_{i,d}(\mathbf{x}) = \sigma_g a(\mathbf{x}) \tanh(B_r(\mathbf{x})^\top \mathbf{w}_{i,d}), \quad \mathbf{w}_{i,d} \sim \mathcal{N}(\mathbf{0}, \mathbf{I}), \quad d \in \{1, 2\},$$

with residual scale σ_g . Here $B_r(\mathbf{x}) = k_r(\mathbf{x}, \mathcal{Z}_r) L^{-\top}$, where \mathcal{Z}_r is a regular inducing grid, $K_{ZZ} + \epsilon I = LL^\top$, and k_r is an anisotropic RBF kernel with lengthscales $(\ell_{r,1}, \ell_{r,2})$. The function

$$a(\mathbf{x}) = \exp \left[-\frac{1}{2} \left(\frac{x_1 - 1.0}{0.85} \right)^2 - \frac{1}{2} \left(\frac{x_2 - 0.9}{0.65} \right)^2 \right]$$

localizes the residual around the typical Lotka–Volterra orbit, which stabilizes the oscillations by damping residual effects away from the observed state region. Thus the shared population field remains mechanistic, while subject deviations are flexible smooth random effects.

C.2 Lotka–Volterra with subject covariates (2D)

This example employed in Section 5.4 uses the same Lotka–Volterra dynamics as above, but the subject-specific interaction coefficients are driven by static covariates. Each subject has $\mathbf{c}_i \in \mathbb{R}^3$ with independent coordinates sampled uniformly from $[-1, 1]$, and

$$\begin{aligned}\dot{x}_{1,i} &= \alpha_0 x_{1,i} - \beta_i x_{1,i} x_{2,i}, \\ \dot{x}_{2,i} &= \delta_i x_{1,i} x_{2,i} - \gamma_0 x_{2,i},\end{aligned}$$

with

$$\beta_i = \beta_0 \exp(\mathbf{w}_\beta^\top \mathbf{c}_i + \sigma_{\text{cov}} \xi_i), \quad \delta_i = \delta_0 \exp(\mathbf{w}_\delta^\top \mathbf{c}_i + \sigma_{\text{cov}} \zeta_i), \quad \xi_i, \zeta_i \sim \mathcal{N}(0, 1).$$

Thus, subjects with nearby covariates have similar interaction rates.

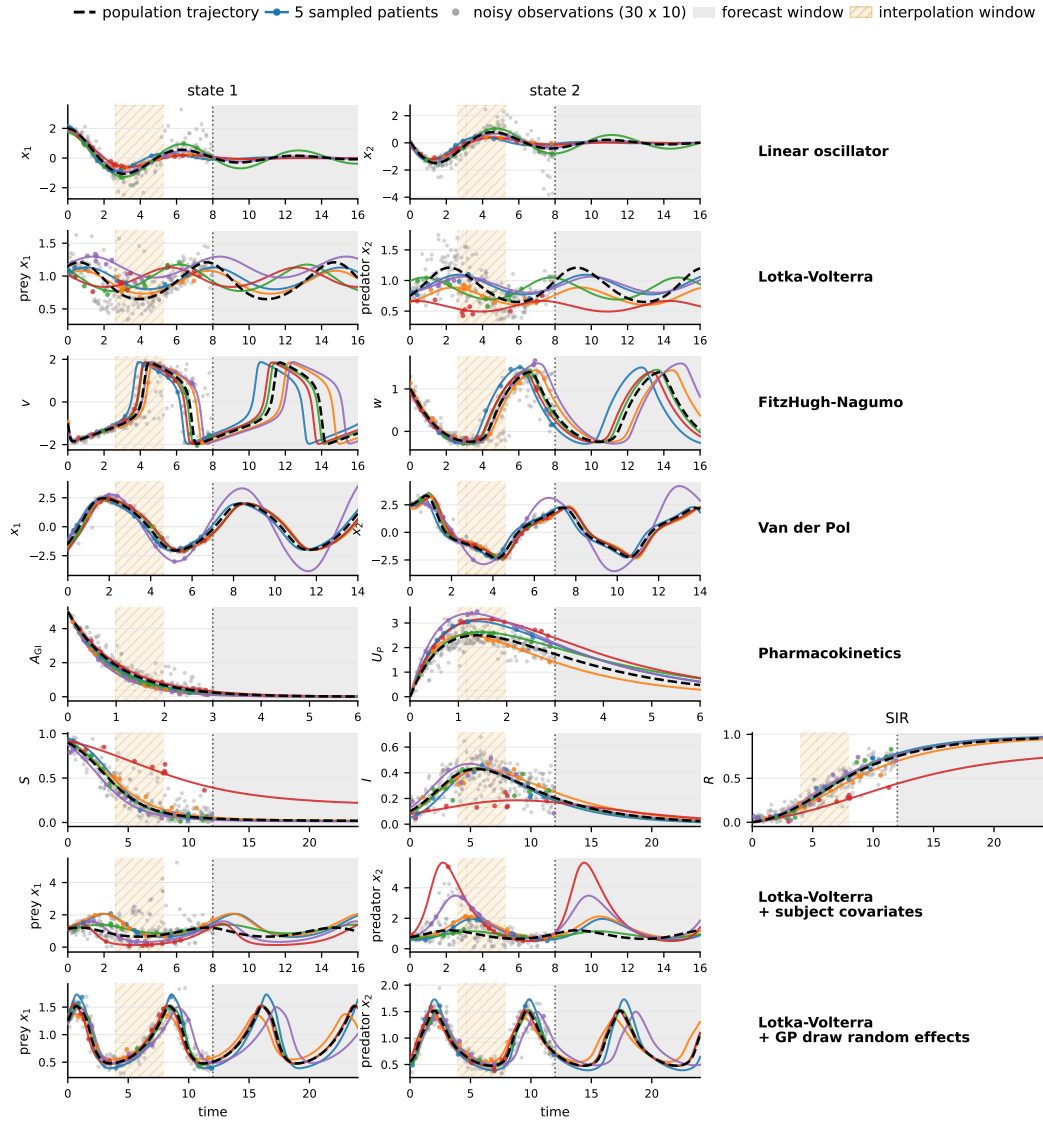


Figure S6: Synthetic benchmark examples used in the experiments. Dashed black curves denote the population trajectory, obtained by integrating the population-only vector field from a single initial condition. Colored curves show five sampled patient trajectories, gray points are noisy observations, and shaded regions indicate interpolation and forecast windows used in the experiments.

C.3 FHN Misspecification Experiment

We include a targeted misspecification experiment to evaluate whether function-space residuals can correct a plausible but incomplete mechanistic ODE. The benchmark starts from the two-dimensional FitzHugh–Nagumo skeleton,

$$\mathbf{f}_{\text{FHN}}(v, w; \boldsymbol{\theta}), \quad \boldsymbol{\theta} = (s, c, I, d, a, b, \tau),$$

but the true population vector field includes an additional smooth state-dependent correction,

$$\mathbf{f}_0^*(\mathbf{x}) = \mathbf{f}_{\text{FHN}}(\mathbf{x}; \boldsymbol{\theta}^*) + \mathbf{h}_0(\mathbf{x}), \quad \mathbf{x} = (v, w).$$

The correction \mathbf{h}_0 is a deterministic bounded RBF/Nyström residual, constructed similarly to the GP-draw random effects in Appendix C, that changes the shape and timing of the oscillations without inducing collapse or blow-up. Subject heterogeneity is then added through small smooth residual fields,

$$\mathbf{f}_i^*(\mathbf{x}) = \mathbf{f}_0^*(\mathbf{x}) + \mathbf{g}_i^*(\mathbf{x}),$$

where each \mathbf{g}_i^* is an independent bounded RBF/Nyström draw.

We compare three methods. First, the mechanistic SAEM baseline of Appendix B.2, which is deliberately doubly misspecified: it fits only a nonlinear mixed-effects FHN model, so it can adjust mechanistic population parameters and parametric random effects, but cannot represent either the shared correction \mathbf{h}_0 or the nonparametric subject-specific residual fields \mathbf{g}_i^* . Standard MEGPODE learns the fully nonparametric decomposition $\mathbf{f}_i = \mathbf{f}_0 + \mathbf{g}_i$ without a mechanistic mean. Finally, MEGPODE-Muses an FHN mean inside the shared field,

$$f_{0,d}(\mathbf{x}) = f_{\text{FHN},d}(\mathbf{x}; \boldsymbol{\theta}) + r_{0,d}(\mathbf{x}),$$

where r_0 is a GP residual and the subject-specific fields \mathbf{g}_i are modeled as in the full method. After each smoothing step, the smoothed derivative pseudo-observations are regressed onto the FHN basis after subtracting the current GP contribution, yielding a weighted ridge least-squares update of $\boldsymbol{\theta}$ with weights given by the collocation uncertainty.

C.4 Hardware

All experiments were conducted on a compute cluster equipped with four NVIDIA V100 GPUs (32 GB memory each), as well as on a MacBook Pro with an Apple M4 Pro chip. Typical synthetic benchmark fits took on the order of minutes using only one CPU core.

D Additional derivations

Notation reference

We begin the section by collecting the notation used in the main text. These are presented below in Tables S3 and S4.

D.1 Derivation of the local Gaussian pseudo-observation

We derive the Gaussian pseudo-observation used in Section 3.3. Starting from the collocation residual in Eq. (16),

$$\mathbf{0} = \mathbf{H}_{\bar{\mathbf{x}}_i,k} \mathbf{s}_{i,k} - \mathbf{f}_i(\mathbf{H}_x \mathbf{s}_{i,k}) + \boldsymbol{\epsilon}_{i,k}^{(\text{coloc})}, \quad \boldsymbol{\epsilon}_{i,k}^{(\text{coloc})} \sim \mathcal{N}(\mathbf{0}, \boldsymbol{\Sigma}_{\text{coloc}}). \quad (\text{S1})$$

We linearize the posterior-mean vector field around a reference point $\bar{\mathbf{x}}_{i,k}$:

$$\mathbb{E}_q[\mathbf{f}_i(\mathbf{H}_x \mathbf{s}_{i,k})] \approx \boldsymbol{\mu}_{i,k}^f + \mathbf{J}_{i,k}(\mathbf{H}_x \mathbf{s}_{i,k} - \bar{\mathbf{x}}_{i,k}), \quad (\text{S2})$$

where

$$\boldsymbol{\mu}_{i,k}^f = \mathbb{E}_q[\mathbf{f}_i(\bar{\mathbf{x}}_{i,k})], \quad \mathbf{J}_{i,k} = \nabla_{\mathbf{x}} \mathbb{E}_q[\mathbf{f}_i(\mathbf{x})] \Big|_{\mathbf{x}=\bar{\mathbf{x}}_{i,k}}. \quad (\text{S3})$$

Symbol	Size	Description	First seen
Observed data and subject-level dynamics			
M	scalar	Number of subjects.	Sec. 2.1
i, n	indices	Subject and within-subject observation indices.	Sec. 2.1
$\mathcal{T}_i = \{t_{i,j}\}_{j=1}^{N_i}$	set	Observation times for subject i .	Sec. 2.1
N_i	scalar	Number of observations for subject i .	Sec. 2.1
D_y	scalar	Observation dimension.	Eq. (1)
D	scalar	Latent-state dimension.	Eq. (1)
$\mathbf{y}_{i,n}$	\mathbb{R}^{D_y}	Observation for subject i at time $t_{i,n}$.	Eq. (1)
$\mathbf{x}_i(t)$	\mathbb{R}^D	Latent state trajectory of subject i .	Eq. (1)
\mathbf{H}	$\mathbb{R}^{D_y \times D}$	Linear observation operator.	Eq. (1)
Σ_y	$\mathbb{R}^{D_y \times D_y}$	Observation-noise covariance.	Eq. (1)
\mathbf{f}_i	$\mathbb{R}^D \rightarrow \mathbb{R}^D$	Subject-specific vector field.	Eq. (2)
$\mathbf{x}_{i,0}$	\mathbb{R}^D	Initial condition for subject i .	Eq. (2)
Mixed-effect field model			
$\mathbf{f}_0, \mathbf{g}_i$	$\mathbb{R}^D \rightarrow \mathbb{R}^D$	Shared population and subject-specific deviation fields.	Eq. (7)
$f_{0,d}, g_{i,d}$	scalar functions	d th coordinates of the shared and local fields.	Eqs. (8)–(9)
k_0, k_r	kernels	GP kernels for the shared and local fields.	Eqs. (8)–(9)
$\mathbf{Z}_0, \mathbf{Z}_r$	$\mathbb{R}^{l_0 \times D}, \mathbb{R}^{l_r \times D}$	Inducing locations for the shared and local fields.	Sec. 3.2
l_0, l_r	scalars	Numbers of shared and local inducing locations.	Sec. 3.2
$\Phi_0(\mathbf{x}), \Phi_r(\mathbf{x})$	$\mathbb{R}^{1 \times l_0}, \mathbb{R}^{1 \times l_r}$	Whitened feature maps for scalable field representation.	Eq. (11)
$\mathbf{b}_{0,d}, \mathbf{b}_{i,d}$	$\mathbb{R}^{l_0}, \mathbb{R}^{l_r}$	Shared and local coefficient vectors for output d .	Eq. (12)
λ_r	scalar	Shrinkage strength for the subject-specific coefficients.	Eq. (13)
$q(\mathbf{b}_{0,d}), q(\mathbf{b}_{i,d})$	Gaussian laws	Variational posteriors over shared and local coefficients.	Sec. 3.2
$\mathbf{m}_{0,d}, \mathbf{m}_{i,d}$	vector	Posterior means of the shared and local coefficients.	Eq. (14)
$\mathbf{S}_{0,d}, \mathbf{S}_{i,d}$	matrix	Posterior covariances of shared and local coefficients.	Eq. (14)

Table S3: Core model and field notation used in the main text.

Substituting Eq. (S2) into Eq. (S1) gives

$$\begin{aligned}
\mathbf{0} &\approx \mathbf{H}_{\dot{x}} \mathbf{s}_{i,k} - \left(\boldsymbol{\mu}_{i,k}^f + \mathbf{J}_{i,k} (\mathbf{H}_x \mathbf{s}_{i,k} - \bar{\mathbf{x}}_{i,k}) \right) + \boldsymbol{\epsilon}_{i,k}^{(\text{coloc})} \\
&= \mathbf{H}_{\dot{x}} \mathbf{s}_{i,k} - \boldsymbol{\mu}_{i,k}^f - \mathbf{J}_{i,k} \mathbf{H}_x \mathbf{s}_{i,k} + \mathbf{J}_{i,k} \bar{\mathbf{x}}_{i,k} + \boldsymbol{\epsilon}_{i,k}^{(\text{coloc})} \\
&= (\mathbf{H}_{\dot{x}} - \mathbf{J}_{i,k} \mathbf{H}_x) \mathbf{s}_{i,k} - (\boldsymbol{\mu}_{i,k}^f - \mathbf{J}_{i,k} \bar{\mathbf{x}}_{i,k}) + \boldsymbol{\epsilon}_{i,k}^{(\text{coloc})}.
\end{aligned} \tag{S4}$$

Rearranging terms yields

$$\boldsymbol{\mu}_{i,k}^f - \mathbf{J}_{i,k} \bar{\mathbf{x}}_{i,k} = (\mathbf{H}_{\dot{x}} - \mathbf{J}_{i,k} \mathbf{H}_x) \mathbf{s}_{i,k} + \boldsymbol{\epsilon}_{i,k}^{(\text{coloc})}. \tag{S5}$$

This is already in linear-Gaussian observation form. Defining

$$\mathbf{H}_{i,k}^{(\text{coloc})} = \mathbf{H}_{\dot{x}} - \mathbf{J}_{i,k} \mathbf{H}_x, \quad \mathbf{c}_{i,k}^{(\text{coloc})} = \boldsymbol{\mu}_{i,k}^f - \mathbf{J}_{i,k} \bar{\mathbf{x}}_{i,k}, \tag{S6}$$

we obtain the pseudo-observation

$$\mathbf{c}_{i,k}^{(\text{coloc})} = \mathbf{H}_{i,k}^{(\text{coloc})} \mathbf{s}_{i,k} + \boldsymbol{\epsilon}_{i,k}, \quad \boldsymbol{\epsilon}_{i,k} \sim \mathcal{N}(\mathbf{0}, \mathbf{R}_{i,k}^{(\text{coloc})}). \tag{S7}$$

Finally, the effective covariance is taken as

$$\mathbf{R}_{i,k}^{(\text{coloc})} = \Sigma_{\text{coloc}} + \Sigma_{i,k}^f, \quad \Sigma_{i,k}^f = \text{Var}_q[\mathbf{f}_i(\bar{\mathbf{x}}_{i,k})], \tag{S8}$$

so that uncertainty in the local field evaluation is incorporated into the pseudo-observation noise.

Strictly speaking, the first-order expansion is applied to the posterior-mean field, while uncertainty in the field evaluation under q is propagated through the additive covariance term $\Sigma_{i,k}^f$. The resulting construction should therefore be understood as a local Gaussian approximation to the random nonlinear term $\mathbf{f}_i(\mathbf{H}_x \mathbf{s}_{i,k})$, rather than as a deterministic plug-in of its posterior mean.

Symbol	Size	Description	First seen
State-space prior and collocation			
$\tau_{i,k}$	scalar	Collocation time for subject i at grid index k .	Eq. (5)
$\mathcal{C}_i = \{\tau_{i,j}\}_{j=1}^{K_i}$	set	Subject-specific collocation grid.	Sec. 3.3
K_i	scalar	Subject-specific collocation grid size.	Sec. 3.3
$\mathbf{s}_{i,k}$	\mathbb{R}^{2D}	Augmented latent state containing $[\mathbf{x}_i(\tau_{i,k}), \dot{\mathbf{x}}_i(\tau_{i,k})]$.	Eq. (5)
$\mathbf{A}(h_k), \mathbf{Q}(h_k)$	matrices	State-transition matrix, process covariance in the state-space GP prior.	Eq. (4)
h_k	scalar	Time step in the state-space GP prior.	Eq. (4)
$\mathbf{H}_x, \mathbf{H}_{\dot{x}}$	$\mathbb{R}^{D \times 2D}$	Selectors extracting state and derivative from $\mathbf{s}_{i,k}$.	Eq. (5)
Σ_{colloc}	$\mathbb{R}^{D \times D}$	Baseline collocation-noise covariance.	Eq. (6)
$\tilde{\mathbf{x}}_{i,k}$	\mathbb{R}^D	Reference point used for local linearization of the collocation factor.	Sec. 3.3
$\boldsymbol{\mu}_{i,k}^f, \Sigma_{i,k}^f$	vector, matrix	Posterior mean and covariance of the subject field evaluated at $\tilde{\mathbf{x}}_{i,k}$.	Eq. (17)
$\mathbf{J}_{i,k}$	matrix	Jacobian of the subject field evaluated at $\tilde{\mathbf{x}}_{i,k}$.	Eq. (17)
$\mathbf{H}_{i,k}^{(\text{colloc})}, \mathbf{c}_{i,k}^{(\text{colloc})}$	matrix, vector	Linearized collocation operator, offset term.	Eqs. (19)–(20)
$\mathbf{R}_{i,k}^{(\text{colloc})}$	matrix	Effective covariance	Eqs. (19)–(20)
$q(\mathbf{s}_{i,0:K_i})$	Gaussian law	Variational posterior over the latent trajectory of subject i on \mathcal{C}_i .	Eq. (15)
Pseudo-data and field regression			
$\tilde{\mathbf{x}}_{i,k}, \tilde{\mathbf{x}}_{i,k}, \tilde{\mathbf{R}}_{i,k}$	vector, vector, matrix	Smoothed pseudo-state, pseudo-derivative, and pseudo-derivative covariance used to refit the field.	Eq. (21)
$\mathbf{u}_{i,d}$	\mathbb{R}^{K_i+1}	Stacked pseudo-derivative targets for subject i , output d .	Eq. (22)
$\mathbf{P}_{0,i,d}, \mathbf{P}_{r,i,d}$	$\mathbb{R}^{(K_i+1) \times l_0}$ $\mathbb{R}^{(K_i+1) \times l_r}$	Shared and local design matrices evaluated at the smoothed states.	Eq. (23)
$\mathbf{R}_{i,d}$	$\mathbb{R}^{(K_i+1) \times (K_i+1)}$	Noise covariance in the pseudo-regression output d .	Eq. (24)
$\boldsymbol{\eta}_{0,d}, \boldsymbol{\eta}_{i,d}$	vector	Natural mean parameters for shared and local Gaussian coefficient posteriors	Eqs. (26)–(28)
$\boldsymbol{\Lambda}_{0,d}, \boldsymbol{\Lambda}_{i,d}$	matrix	Natural precision for the shared and local Gaussian coefficient posteriors.	Eqs. (25)–(27)

Table S4: Trajectory, collocation, and inference notation used in the main text.

D.2 Trajectory-space Kalman smoothing update

Once the collocation pseudo-observation $\mathbf{c}_{i,k}^{(\text{colloc})}$ in Eq. (19) in the main text is locally linearized, each subject-specific trajectory posterior is updated in a linear-Gaussian state-space model. Recall the Gauss–Markov prior from Eq. (4)

$$\mathbf{s}_{i,k+1} = \mathbf{A}_{i,k} \mathbf{s}_{i,k} + \mathbf{q}_{i,k}, \quad \mathbf{q}_{i,k} \sim \mathcal{N}(\mathbf{0}, \mathbf{Q}_{i,k}), \quad (\text{S9})$$

with $\mathbf{s}_{i,k+1}$ from Eq. (5). At each collocation time $\tau_{i,k}$, define the stacked observation vector

$$\mathbf{w}_{i,k} = \begin{cases} \begin{bmatrix} \mathbf{y}_{i,k} \\ \mathbf{c}_{i,k}^{(\text{colloc})} \end{bmatrix}, & \text{if } \tau_{i,k} \text{ is an observation time,} \\ \mathbf{c}_{i,k}^{(\text{colloc})}, & \text{otherwise,} \end{cases} \quad (\text{S10})$$

where $\mathbf{y}_{i,k}$ is the physical observation from Eq. (1). The corresponding linear operator is

$$\mathbf{H}_{i,k}^{(\text{smooth})} = \begin{cases} \begin{bmatrix} \mathbf{H}\mathbf{H}_x \\ \mathbf{H}_{i,k}^{(\text{colloc})} \end{bmatrix}, & \text{if } \tau_{i,k} \text{ is an observation time,} \\ \mathbf{H}_{i,k}^{(\text{colloc})}, & \text{otherwise.} \end{cases} \quad (\text{S11})$$

Here $\mathbf{H}\mathbf{H}_x \in \mathbb{R}^{D_y \times 2D}$ maps the augmented state $\mathbf{s}_{i,k}$ to the physical observation space, while $\mathbf{H}_{i,k}^{(\text{colloc})} \in \mathbb{R}^{D \times 2D}$ is the linearized collocation operator from Eq. (20). where \mathbf{H} comes from the

observation model in Eq. (1) and $\mathbf{H}_{i,k}^{(\text{coloc})}$ from Eq. (20). The associated block noise covariance is

$$\mathbf{S}_{i,k}^{\text{obs}} = \begin{cases} \begin{bmatrix} \Sigma_{i,k}^y & \mathbf{0} \\ \mathbf{0} & \mathbf{R}_{i,k}^{(\text{coloc})} \end{bmatrix}, & \text{if } \tau_{i,k} \text{ is an observation time,} \\ \mathbf{R}_{i,k}^{(\text{coloc})}, & \text{otherwise,} \end{cases} \quad (\text{S12})$$

where $\Sigma_{i,k}^y$ denotes the observation-noise covariance at grid point $\tau_{i,k}$. In the homoscedastic setting of Eq. (1), this reduces to $\Sigma_{i,k}^y \equiv \Sigma_y$. Then

$$\mathbf{w}_{i,k} = \mathbf{H}_{i,k}^{(\text{smooth})} \mathbf{s}_{i,k} + \mathbf{r}_{i,k}, \quad \mathbf{r}_{i,k} \sim \mathcal{N}(\mathbf{0}, \mathbf{S}_{i,k}^{\text{obs}}). \quad (\text{S13})$$

Filtering yields forward marginals

$$p(\mathbf{s}_{i,k} \mid \mathbf{w}_{i,0:k}) = \mathcal{N}(\boldsymbol{\mu}_{i,k}^{\text{flt}}, \boldsymbol{\Sigma}_{i,k}^{\text{flt}}), \quad (\text{S14})$$

and the backward smoothing pass yields smoothed marginals

$$q(\mathbf{s}_{i,k}) = \mathcal{N}(\boldsymbol{\mu}_{i,k}^{\text{smooth}}, \boldsymbol{\Sigma}_{i,k}^{\text{smooth}}) \quad (\text{S15})$$

together with lag-one cross-covariances of the form

$$\text{Cov}(\mathbf{s}_{i,k}, \mathbf{s}_{i,k+1} \mid \mathbf{w}_{i,0:K_i}), \quad (\text{S16})$$

which are needed when working with the full joint Gaussian Markov posterior over the trajectory. Standard linear-Gaussian filtering and smoothing recursions therefore apply directly [32]. For further details on state-space GP inference and Kalman smoothing, see Särkkä and Solin [33], Tronarp et al. [38].

D.3 Extrapolation for a trained subject

Suppose subject i is part of the training set and that, after training on observations in $[0, T_{\text{obs}}]$, we have learned the shared and subject-specific posteriors

$$q(\mathbf{b}_{0,d}) = \mathcal{N}(\mathbf{m}_{0,d}, \mathbf{S}_{0,d}), \quad q(\mathbf{b}_{i,d}) = \mathcal{N}(\mathbf{m}_{i,d}, \mathbf{S}_{i,d}), \quad d = 1, \dots, D.$$

To extrapolate this same subject to a longer horizon $T_{\text{pred}} > T_{\text{obs}}$, we freeze the learned field posterior and recompute only the trajectory posterior on an extended collocation grid.

Let

$$\mathcal{C}_i^{\text{pred}} = \{\tau_{i,0}, \dots, \tau_{i,K_i^{\text{pred}}}\}$$

be a collocation grid such that

$$\mathcal{C}_i^{\text{obs}} \subseteq \mathcal{C}_i^{\text{pred}}, \quad \max \mathcal{C}_i^{\text{pred}} = T_{\text{pred}},$$

where $\mathcal{C}_i^{\text{obs}}$ is the grid used during training on $[0, T_{\text{obs}}]$. On this extended grid we keep the original physical observations on $[0, T_{\text{obs}}]$ and treat all later grid points as unobserved.

The target of extrapolation is therefore the extended trajectory posterior

$$q\left(\mathbf{s}_{i,0:K_i^{\text{pred}}} \mid \mathbf{y}_i(0:T_{\text{obs}}), q(\mathbf{b}_0), q(\mathbf{b}_i)\right),$$

whose marginal over $\tau_{i,k} \in [T_{\text{obs}}, T_{\text{pred}}]$ yields the forecast.

Since the field posterior is fixed, extrapolation reuses the same local-linearization and Kalman-smoothing construction as in Section 3.3 and Appendix D.2, but on the enlarged grid $\mathcal{C}_i^{\text{pred}}$. It is a *trajectory-only* inference step: the field is frozen, and the latent path is recomputed jointly on $[0, T_{\text{pred}}]$, with no physical observations beyond T_{obs} . Thus, it is not a simple forward rollout from an estimate at T_{obs} , and enlarging the horizon may slightly modify the posterior even on the observed interval.

For `f0_only`, the same extrapolation procedure is used with $\mathbf{g}_i \equiv \mathbf{0}$, so prediction is driven only by the shared field. For `gi_only`, the shared component is absent and extrapolation uses only the trained subject-specific field of subject i .

D.4 Adaptation and extrapolation for a new subject after training

Suppose training has produced shared posteriors

$$q(\mathbf{b}_{0,d}) = \mathcal{N}(\mathbf{m}_{0,d}, \mathbf{S}_{0,d}), \quad d = 1, \dots, D.$$

For a new subject \star , we keep the shared field fixed and infer only a new local posterior $q(\mathbf{b}_{\star,d})$ together with the subject trajectory posterior on the observed window. Let

$$\mathcal{C}_{\star}^{\text{obs}} = \{\tau_{\star,0}, \dots, \tau_{\star,K_{\star}}\}$$

denote a collocation grid covering the available observations.

Adaptation reuses the same trajectory-space update of Section 3.3 and the same pseudo-regression construction of Section 3.4, except that the shared posterior is held fixed and only the subject-specific posterior is updated. For output dimension d , the personalized pseudo-regression is

$$\mathbf{u}_{\star,d} = \mathbf{P}_{0,\star,d} \mathbf{b}_{0,d} + \mathbf{P}_{r,\star,d} \mathbf{b}_{\star,d} + \boldsymbol{\varepsilon}_{\star,d}^{\text{reg}}, \quad \boldsymbol{\varepsilon}_{\star,d}^{\text{reg}} \sim \mathcal{N}(\mathbf{0}, \mathbf{R}_{\star,d}), \quad (\text{S17})$$

which yields the local natural-parameter update

$$\boldsymbol{\Lambda}_{\star,d}^{\text{new}} = \lambda_r \mathbf{I}_{l_r} + \mathbf{P}_{r,\star,d}^{\top} \mathbf{R}_{\star,d}^{-1} \mathbf{P}_{r,\star,d}, \quad (\text{S18})$$

$$\boldsymbol{\eta}_{\star,d}^{\text{new}} = \mathbf{P}_{r,\star,d}^{\top} \mathbf{R}_{\star,d}^{-1} (\mathbf{u}_{\star,d} - \mathbf{P}_{0,\star,d} \mathbf{m}_{0,d}). \quad (\text{S19})$$

Thus adaptation is an alternating scheme in which the shared field remains fixed, while the new subject trajectory and local field are refined jointly.

When $N_{\star} = 0$, the procedure reduces to a population-only forecast by keeping $\mathbf{m}_{\star,d} = \mathbf{0}$. When only an early prefix is observed, the same algorithm yields few-shot personalization.

For `f0_only`, the local update is omitted entirely. For `gi_only`, the shared component is absent and only the subject-specific field is adapted.

D.5 Initial conditions

We treat the initial condition as a latent subject-specific quantity and place a simple mixed-effect Gaussian prior on it. Let $\tau_{i,0}$ denote the left endpoint of the collocation grid for subject i (typically $\tau_{i,0} = 0$), and write

$$\mathbf{x}_{i,0} := \mathbf{x}_i(\tau_{i,0}).$$

We model

$$\mathbf{x}_{i,0} = \boldsymbol{\mu}_{x_0} + \mathbf{a}_i, \quad \mathbf{a}_i \sim \mathcal{N}(\mathbf{0}, \boldsymbol{\Sigma}_{x_0}), \quad i = 1, \dots, M. \quad (\text{S20})$$

Thus $\boldsymbol{\mu}_{x_0}$ is a population reference initial state and $\boldsymbol{\Sigma}_{x_0}$ captures between-subject variability at the initial time.

Initial prior in the augmented state-space model. The smoother operates on the augmented state

$$\mathbf{s}_{i,k} = \begin{bmatrix} \mathbf{x}_i(\tau_{i,k}) \\ \dot{\mathbf{x}}_i(\tau_{i,k}) \end{bmatrix}.$$

The mixed-effect initial-condition prior is applied only to the state block of $\mathbf{s}_{i,0}$, while the derivative block remains under the default temporal prior. Concretely, the initial Gaussian prior has the form

$$\mathbf{s}_{i,0} \sim \mathcal{N}\left(\begin{bmatrix} \boldsymbol{\mu}_{x_0} \\ \mathbf{0} \end{bmatrix}, \begin{bmatrix} \boldsymbol{\Sigma}_{x_0} & \mathbf{0} \\ \mathbf{0} & \mathbf{P}_{\dot{x},0} \end{bmatrix}\right), \quad (\text{S21})$$

where $\mathbf{P}_{\dot{x},0}$ is the default prior covariance for the initial derivative coordinates. Hence the model learns a population prior for $\mathbf{x}_{i,0}$, while $\dot{\mathbf{x}}_i(\tau_{i,0})$ is inferred indirectly through the observations and collocation constraints.

Empirical-Bayes initialization. For simplicity, we describe the empirical initialization used in the fully observed case, where $D_y = D$ and $\mathbf{H} = \mathbf{I}_D$. Because the observation times are irregular and need not include $\tau_{i,0}$, we initialize the population initial-condition model from the earliest observed state of each subject. Let $\mathbf{y}_{i,(1)}$ denote the first observed state vector for subject i . The initialization is

$$\boldsymbol{\mu}_{x_0}^{(0)} = \frac{1}{M} \sum_{i=1}^M \mathbf{y}_{i,(1)}, \quad (\text{S22})$$

$$\boldsymbol{\Sigma}_{x_0}^{(0)} = \alpha_{x_0} \widehat{\text{Cov}}(\mathbf{y}_{1,(1)}, \dots, \mathbf{y}_{M,(1)}) + \epsilon_{x_0} \mathbf{I}_D, \quad (\text{S23})$$

where $\alpha_{x_0} > 0$ is a scale factor and $\epsilon_{x_0} > 0$ is a small jitter term. For partially observed settings with $D_y < D$, one must first map or impute the first observations into the latent state space before forming $\boldsymbol{\mu}_{x_0}^{(0)}$ and $\boldsymbol{\Sigma}_{x_0}^{(0)}$. This is only an initialization heuristic: when the first observation occurs after $\tau_{i,0}$, it is not itself the true initial state, but it provides a reasonable empirical anchor from which the smoother can refine $\mathbf{x}_{i,0}$.

Update after each smoothing step. After smoothing all subjects with the current field posterior, we extract the smoothed marginal at the first grid point,

$$q(\mathbf{x}_{i,0}) = \mathcal{N}(\mathbf{m}_{i,0}^x, \mathbf{P}_{i,0}^{xx}),$$

and update the population initial-condition parameters by moment matching:

$$\boldsymbol{\mu}_{x_0}^{\text{new}} = \frac{1}{M} \sum_{i=1}^M \mathbf{m}_{i,0}^x, \quad (\text{S24})$$

$$\boldsymbol{\Sigma}_{x_0}^{\text{new}} = \frac{1}{M} \sum_{i=1}^M \left[\mathbf{P}_{i,0}^{xx} + (\mathbf{m}_{i,0}^x - \boldsymbol{\mu}_{x_0}^{\text{new}})(\mathbf{m}_{i,0}^x - \boldsymbol{\mu}_{x_0}^{\text{new}})^\top \right] + \epsilon_{x_0} \mathbf{I}_D. \quad (\text{S25})$$

Hence the initial-condition layer is updated in an EM-like empirical-Bayes fashion: smoothing provides posterior moments for the subject-specific initial states, and these are pooled to refresh the population-level prior before the next outer iteration.

Initialization of the trajectory linearization. The current trajectory linearization is initialized from an observation-only Gaussian smoothing pass under the current initial-condition prior. If $q^{(0)}(\mathbf{s}_{i,0:K_i})$ denotes this initial observation-only posterior, then the initial reference trajectory used by the collocation linearization is

$$\bar{\mathbf{x}}_{i,k}^{(0)} := \mathbb{E}_{q^{(0)}}[\mathbf{x}_i(\tau_{i,k})]. \quad (\text{S26})$$

Thus the initial-condition prior influences the outer linearization through the initial observation-driven smoothing step.

Population mean versus subject-specific initial conditions. This construction yields two distinct quantities.

First, the *population reference initial condition* is the learned mean $\mathbf{x}_0^{\text{pop}} := \boldsymbol{\mu}_{x_0}$. This is the natural initial state for propagating the shared population field and obtaining a population mean trajectory.

Second, for a given subject i , the relevant initial-condition summary after training is the subject-specific smoothed posterior

$$q(\mathbf{x}_{i,0}) = \mathcal{N}(\mathbf{m}_{i,0}^x, \mathbf{P}_{i,0}^{xx}).$$

Thus the population prior regularizes the estimation of $\mathbf{x}_{i,0}$, but the final subject-level initial condition remains individualized by the data and the inferred subject-specific dynamics.

Baselines. The same initial-condition mechanism is used for the full mixed-effect model and for the two ablations `f0_only` and `gi_only`. The differences between methods only concern the vector-field layer.

D.6 Hyperparameter learning

We learn hyperparameters via empirical-Bayes updates after the current smoothing pass. Recall that the smoothed trajectories define pseudo-regression targets for the vector field (Equation 24),

$$\mathbf{u}_{i,d} = \mathbf{P}_{0,i,d}\mathbf{b}_{0,d} + \mathbf{P}_{r,i,d}\mathbf{b}_{i,d} + \boldsymbol{\varepsilon}_{i,d}, \quad \boldsymbol{\varepsilon}_{i,d} \sim \mathcal{N}(0, \mathbf{R}_{i,d}).$$

The kernel hyperparameters and field output scales, denoted collectively by θ , are chosen by minimizing the marginal negative log likelihood of these pseudo-data after integrating out the Gaussian field weights:

$$\mathcal{L}_{\text{field}}(\theta) = - \sum_{d=1}^D \log \int p_{\theta}(\{\mathbf{u}_{i,d}\}_i \mid \mathbf{b}_{0,d}, \{\mathbf{b}_{i,d}\}_i) p(\mathbf{b}_{0,d}) \prod_i p_{\lambda_r}(\mathbf{b}_{i,d}) d\mathbf{b}_{0,d} \prod_i d\mathbf{b}_{i,d}. \quad (\text{S27})$$

The observation noise is updated from the smoothing posterior moments. If $\mathbf{m}_{i,k}$ and $\mathbf{S}_{i,k}$ are the smoothed mean and covariance at an observed time, then

$$\hat{\sigma}_y^2 = \frac{1}{N_{\text{obs}}} \sum_{(i,k,a) \in \mathcal{O}} \left[(y_{i,k,a} - (\mathbf{H}\mathbf{m}_{i,k})_a)^2 + (\mathbf{H}\mathbf{S}_{i,k}\mathbf{H}^{\top})_{aa} \right]. \quad (\text{S28})$$

Similarly, writing the IWP transition covariance as $\mathbf{Q}(h) = \sigma_{\text{IWP}}^2 \mathbf{Q}_0(h)$, the process scale is updated by

$$\hat{\sigma}_{\text{IWP}}^2 = \frac{1}{N_q} \sum_{i,k} \text{tr}[\mathbf{Q}_0(h_k)^{-1} \mathbb{E}[\boldsymbol{\varepsilon}_{i,k}\boldsymbol{\varepsilon}_{i,k}^{\top}]], \quad \boldsymbol{\varepsilon}_{i,k} = \mathbf{s}_{i,k+1} - \mathbf{A}(h_k)\mathbf{s}_{i,k}. \quad (\text{S29})$$

Finally, the residual precision λ_r is updated from the posterior moments of the subject-specific field weights. With Gamma prior parameters $(a_{\lambda}, b_{\lambda})$,

$$\hat{\lambda}_r = \frac{a_{\lambda} - 1 + \frac{1}{2}MDl_r}{b_{\lambda} + \frac{1}{2} \sum_{i,d} (\|\mathbb{E}[\mathbf{b}_{i,d}]\|^2 + \text{tr Var}[\mathbf{b}_{i,d}])}. \quad (\text{S30})$$

D.7 Field-space updates and conservative shared-field variants

The main-text update uses a plug-in approximation in which the vector field is regressed on smoothed state means. For vector-valued states, one may either retain the full block covariance of the pseudo-derivatives or use a diagonal approximation separately for each output dimension. The latter leads to the regression form in Eq. (24).

Two conservative variants are useful when updating the shared field. In the *diagonal-inflated* update, the noise covariance for the shared-field regression is augmented by the posterior variance of the local field evaluated at the smoothed inputs:

$$\mathbf{R}_{i,d}^{\text{infl}} = \mathbf{R}_{i,d} + \text{diag}(\text{Var}_q[g_{i,d}(\tilde{\mathbf{x}}_{i,0})], \dots, \text{Var}_q[g_{i,d}(\tilde{\mathbf{x}}_{i,K_i})]). \quad (\text{S31})$$

This discourages the population field from explaining variability that could plausibly be attributed to an uncertain local effect.

In the *posterior-collapsed* update, the shared-field regression accounts for uncertainty in the current local variational posterior by inflating the pseudo-regression covariance:

$$\boldsymbol{\Sigma}_{i,d}^{\text{coll}} = \mathbf{R}_{i,d} + \mathbf{P}_{r,i,d}\mathbf{S}_{i,d}\mathbf{P}_{r,i,d}^{\top}.$$

The shared-field candidate update becomes

$$\boldsymbol{\Lambda}_{0,d}^{\text{new,coll}} = \mathbf{I}_{l_0} + \sum_{i=1}^M \mathbf{P}_{0,i,d}^{\top} (\boldsymbol{\Sigma}_{i,d}^{\text{coll}})^{-1} \mathbf{P}_{0,i,d}, \quad (\text{S32})$$

$$\boldsymbol{\eta}_{0,d}^{\text{new,coll}} = \sum_{i=1}^M \mathbf{P}_{0,i,d}^{\top} (\boldsymbol{\Sigma}_{i,d}^{\text{coll}})^{-1} (\mathbf{u}_{i,d} - \mathbf{P}_{r,i,d}\mathbf{m}_{i,d}). \quad (\text{S33})$$

Hence uncertainty in the local field is propagated into the shared-field update through the inflated covariance $\boldsymbol{\Sigma}_{i,d}^{\text{coll}}$, making this update more conservative when estimating the population field. We used the collapsed updates in the experiments.

D.8 Population trajectory uncertainty via Monte Carlo pushforward

A derived quantity of interest is the population trajectory obtained by integrating the shared population field from a reference initial condition. In the current implementation, uncertainty over this trajectory is approximated by Monte Carlo pushforward.

Concretely, we draw samples from the learned uncertainty in the population-level dynamics and propagate each sample through the ODE to obtain a collection of population trajectories. Pointwise posterior summaries, such as means, intervals, NLPD, and CRPS, are then computed from this ensemble of simulated trajectories.

D.9 Static subject covariates

For static covariates \mathbf{c}_i , a convenient extension is to keep the state-space inducing features $\Phi_r(\mathbf{x})$ and to correlate the subject-specific coefficient vectors across subjects via a covariate kernel. For each output dimension d , stack the local coefficients as

$$\boldsymbol{\beta}_d = \begin{bmatrix} \mathbf{b}_{1,d} \\ \vdots \\ \mathbf{b}_{M,d} \end{bmatrix} \in \mathbb{R}^{Ml_r}, \quad [K_c]_{ij} = k_c(\mathbf{c}_i, \mathbf{c}_j),$$

and replace the independent prior in Eq. (13) by

$$\boldsymbol{\beta}_d \sim \mathcal{N}(\mathbf{0}, K_c \otimes \lambda_r^{-1} \mathbf{I}_{l_r}).$$

Equivalently,

$$\text{Cov}(\mathbf{b}_{i,d}, \mathbf{b}_{j,d}) = k_c(\mathbf{c}_i, \mathbf{c}_j) \lambda_r^{-1} \mathbf{I}_{l_r}.$$

Retaining $g_{i,d}(\mathbf{x}) = \Phi_r(\mathbf{x}) \mathbf{b}_{i,d}$, we then have

$$\text{Cov}[g_{i,d}(\mathbf{x}), g_{j,d}(\mathbf{x}')] = \lambda_r^{-1} k_c(\mathbf{c}_i, \mathbf{c}_j) \Phi_r(\mathbf{x}) \Phi_r(\mathbf{x}')^\top,$$

which is precisely the finite-rank approximation of the product kernel on augmented inputs,

$$k_{\text{aug}}((\mathbf{x}, \mathbf{c}_i), (\mathbf{x}', \mathbf{c}_j)) = k_r(\mathbf{x}, \mathbf{x}') k_c(\mathbf{c}_i, \mathbf{c}_j).$$

This is usually preferable to introducing subject-specific kernels k_{r_i} , because k_{r_i} changes each subject marginally but does not by itself encode how two subjects with similar covariates should borrow strength. The covariate Gram matrix K_c is static, so it can be precomputed once, and no inducing locations in covariate space are required. Prediction for a new subject with covariates \mathbf{c}_* only requires the cross-covariance vector $(k_c(\mathbf{c}_*, \mathbf{c}_1), \dots, k_c(\mathbf{c}_*, \mathbf{c}_M))$.

If the covariates are mixed continuous/discrete, k_c can itself be a product or sum of kernels over the continuous and discrete parts.

E Theoretical properties

This section develops a set of structural properties of the proposed mixed-effect GP-ODE model. These results clarify three aspects of the framework: the well-posedness and trajectory-level implications of the posterior-mean dynamics, the covariance and uncertainty structure induced by the hierarchical function-space decomposition, and the exact Gaussian geometry of the conditional field-update subproblem once smoothed pseudo-data are fixed. Table S5 provides an overview of the results. The proofs ultimately draw on standard results from ODEs [37], Gaussian linear models [3], Gaussian processes [30], and their state-space representation [33], and matrix analysis/convex optimization [4].

E.1 Posterior-mean dynamics: well-posedness and trajectory-level deviation bounds

Recall that the posterior-mean shared and subject-specific fields are

$$\bar{\mathbf{f}}_{0,d}(\mathbf{x}) = \Phi_0(\mathbf{x}) \mathbf{m}_{0,d}, \quad \bar{\mathbf{g}}_{i,d}(\mathbf{x}) = \Phi_r(\mathbf{x}) \mathbf{m}_{i,d}, \quad \bar{\mathbf{f}}_{i,d}(\mathbf{x}) = \bar{\mathbf{f}}_{0,d}(\mathbf{x}) + \bar{\mathbf{g}}_{i,d}(\mathbf{x}), \quad (\text{S34})$$

and define the corresponding vector fields

$$\bar{\mathbf{f}}_0(\mathbf{x}) = [\bar{\mathbf{f}}_{0,d}(\mathbf{x})]_{d=1}^D, \quad \bar{\mathbf{g}}_i(\mathbf{x}) = [\bar{\mathbf{g}}_{i,d}(\mathbf{x})]_{d=1}^D, \quad \bar{\mathbf{f}}_i(\mathbf{x}) = \bar{\mathbf{f}}_0(\mathbf{x}) + \bar{\mathbf{g}}_i(\mathbf{x}). \quad (\text{S35})$$

These are the deterministic fields obtained by integrating posterior means in the main text when simulating population and subject-level trajectories.

Theme	Representative statement	Practical takeaway
Posterior-mean dynamics for simulation and summary		
Posterior-mean ODEs (Proposition 1)	For C^1 feature maps, the posterior-mean shared and subject-specific fields define well-posed trajectories.	Justifies summary statistics based on numerically integrating posterior-mean patient and population fields.
Trajectory deviation bound (Proposition 2)	The gap between a subject-level and population-level posterior-mean trajectory is controlled by the size of the local field.	Makes the dynamical effect of heterogeneity explicit: small local fields imply trajectories stay close to the population reference.
Exact structural properties of the hierarchical field model		
Cross-subject covariance (Proposition 3)	The prior covariance splits into shared population terms and within-subject residual terms, yielding an explicit same-input cross-subject correlation.	Gives the function-space analogue of the classical population + random-effect decomposition and clarifies the role of λ_r .
Predictive uncertainty split (Propositions 4 and 5)	At fixed state inputs, predictive variance splits into population and local parts. For trajectory functionals, exact total-variance and first-order pushforward decompositions exist.	Provides diagnostics for whether uncertainty is driven primarily by population estimation or by subject-specific adaptation.
Conditionally exact properties of the Gaussian field subproblem		
Weighted mixed ridge regression (Proposition 6; Corollary 8)	Once smoothed pseudo-derivatives are fixed, the field update is exactly a heteroscedastic mixed ridge regression in feature space.	Clarifies what the alternating algorithm solves.
Conditional uniqueness (Corollary 7)	The conditional field objective is strictly convex; both the joint optimum and each block update are unique.	Rules out ambiguity between shared and local terms once the current pseudo-data are fixed.
Spectral shrinkage (Proposition 9)	Local adaptation shrinks along weighted singular directions.	Makes the role of λ_r explicit.
Monotone information accumulation (Proposition 10)	Adding subjects increases shared precision and decreases shared covariance.	Formalizes borrowing of strength and mirrors the precision-addition structure of MAGMA [19].

Table S5: Overview of the theoretical properties for the proposed MEGPODE.

Proposition 1 (Well-posedness of posterior-mean dynamics). *Assume that the feature maps Φ_0 and Φ_r are continuously differentiable on an open domain $\mathcal{D} \subset \mathbb{R}^D$. Then $\bar{\mathbf{f}}_0$, $\bar{\mathbf{g}}_i$, and $\bar{\mathbf{f}}_i$ are continuously differentiable on \mathcal{D} and hence locally Lipschitz. Consequently, for any initial condition $\mathbf{x}^* \in \mathcal{D}$, the ODEs*

$$\dot{\mathbf{x}}(t) = \bar{\mathbf{f}}_0(\mathbf{x}(t)), \quad \dot{\mathbf{x}}(t) = \bar{\mathbf{f}}_i(\mathbf{x}(t)) \quad (\text{S36})$$

admit unique maximal solutions. In particular, integrating posterior-mean fields to obtain population or subject-level trajectory summaries is mathematically well-defined on any time interval on which the solution remains in \mathcal{D} .

Proof. Each coordinate of $\bar{\mathbf{f}}_0$ is of the form $\mathbf{x} \mapsto \Phi_0(\mathbf{x})\mathbf{m}_{0,d}$, and each coordinate of $\bar{\mathbf{g}}_i$ is of the form $\mathbf{x} \mapsto \Phi_r(\mathbf{x})\mathbf{m}_{i,d}$. Since Φ_0 and Φ_r are C^1 , so are these coordinate functions, and therefore $\bar{\mathbf{f}}_0$, $\bar{\mathbf{g}}_i$, and $\bar{\mathbf{f}}_i$ are C^1 . Every C^1 map is locally Lipschitz, so the standard Picard–Lindelöf theorem yields unique maximal solutions for the corresponding ODEs. \square

The next result quantifies how the norm of the subject-specific residual field controls the departure between a subject trajectory and the corresponding population trajectory.

Proposition 2 (Trajectory deviation controlled by the local field). *Let $\bar{\mathbf{x}}_0 : [0, T] \rightarrow \mathbb{R}^D$ solve*

$$\dot{\bar{\mathbf{x}}}_0(t) = \bar{\mathbf{f}}_0(\bar{\mathbf{x}}_0(t)), \quad \bar{\mathbf{x}}_0(0) = \mathbf{x}_0^*, \quad (\text{S37})$$

and let $\bar{\mathbf{x}}_i : [0, T] \rightarrow \mathbb{R}^D$ solve

$$\dot{\bar{\mathbf{x}}}_i(t) = \bar{\mathbf{f}}_i(\bar{\mathbf{x}}_i(t)) = \bar{\mathbf{f}}_0(\bar{\mathbf{x}}_i(t)) + \bar{\mathbf{g}}_i(\bar{\mathbf{x}}_i(t)), \quad \bar{\mathbf{x}}_i(0) = \mathbf{x}_i^*. \quad (\text{S38})$$

Assume that both trajectories remain in a compact set $\mathcal{K} \subset \mathcal{D}$ on which $\bar{\mathbf{f}}_0$ is L -Lipschitz, and define

$$\delta_i := \sup_{\mathbf{x} \in \mathcal{K}} \|\bar{\mathbf{g}}_i(\mathbf{x})\|. \quad (\text{S39})$$

Then, for every $t \in [0, T]$,

$$\|\bar{\mathbf{x}}_i(t) - \bar{\mathbf{x}}_0(t)\| \leq e^{Lt} \|\mathbf{x}_i^* - \mathbf{x}_0^*\| + \int_0^t e^{L(t-s)} \|\bar{\mathbf{g}}_i(\bar{\mathbf{x}}_i(s))\| ds \leq e^{Lt} \|\mathbf{x}_i^* - \mathbf{x}_0^*\| + \frac{\delta_i}{L} (e^{Lt} - 1) \quad (\text{S40})$$

when $L > 0$, with the usual limit $\|\mathbf{x}_i^* - \mathbf{x}_0^*\| + \delta_i t$ when $L = 0$. In particular, if $\mathbf{x}_i^* = \mathbf{x}_0^*$, then

$$\|\bar{\mathbf{x}}_i(t) - \bar{\mathbf{x}}_0(t)\| \leq \frac{\delta_i}{L} (e^{Lt} - 1). \quad (\text{S41})$$

Proof. Let $\Delta_i(t) = \bar{\mathbf{x}}_i(t) - \bar{\mathbf{x}}_0(t)$. Then

$$\dot{\Delta}_i(t) = \bar{\mathbf{f}}_0(\bar{\mathbf{x}}_i(t)) - \bar{\mathbf{f}}_0(\bar{\mathbf{x}}_0(t)) + \bar{\mathbf{g}}_i(\bar{\mathbf{x}}_i(t)). \quad (\text{S42})$$

Taking norms and using the Lipschitz property of $\bar{\mathbf{f}}_0$ gives

$$\frac{d}{dt} \|\Delta_i(t)\| \leq L \|\Delta_i(t)\| + \|\bar{\mathbf{g}}_i(\bar{\mathbf{x}}_i(t))\|. \quad (\text{S43})$$

Applying Grönwall's inequality yields

$$\|\Delta_i(t)\| \leq e^{Lt} \|\Delta_i(0)\| + \int_0^t e^{L(t-s)} \|\bar{\mathbf{g}}_i(\bar{\mathbf{x}}_i(s))\| ds, \quad (\text{S44})$$

and the uniform bound by δ_i gives Eq. (S40). \square

Propositions 1 and 2 justify the common practice of integrating posterior-mean shared and subject-specific fields to summarize population and patient-level trajectories. In particular, the second result shows that the magnitude of the learned local field directly controls how far subject-specific posterior-mean trajectories can depart from the population one.

E.2 Hierarchical field covariance and predictive uncertainty decompositions

The next statements are exact consequences of the hierarchical function-space decomposition used by the model. They do not depend on the collocation approximation or on the alternating inference scheme.

Proposition 3 (Cross-subject covariance and same-input cross-subject correlation). *Fix an output dimension d . Under the prior field decomposition*

$$f_{i,d}(\mathbf{x}) = \Phi_0(\mathbf{x})\mathbf{b}_{0,d} + \Phi_r(\mathbf{x})\mathbf{b}_{i,d}, \quad \mathbf{b}_{0,d} \sim \mathcal{N}(\mathbf{0}, \mathbf{I}_{l_0}), \quad \mathbf{b}_{i,d} \sim \mathcal{N}(\mathbf{0}, \lambda_r^{-1} \mathbf{I}_{l_r}), \quad (\text{S45})$$

with all coefficients independent across subjects and output dimensions, define

$$\kappa_0(\mathbf{x}, \mathbf{x}') := \Phi_0(\mathbf{x})\Phi_0(\mathbf{x}')^\top, \quad \kappa_r(\mathbf{x}, \mathbf{x}') := \lambda_r^{-1} \Phi_r(\mathbf{x})\Phi_r(\mathbf{x}')^\top. \quad (\text{S46})$$

Then for any subjects i, j , outputs d, d' , and inputs \mathbf{x}, \mathbf{x}' ,

$$\text{Cov}(f_{i,d}(\mathbf{x}), f_{j,d'}(\mathbf{x}')) = \mathbb{I}\{d = d'\} \left(\kappa_0(\mathbf{x}, \mathbf{x}') + \mathbb{I}\{i = j\} \kappa_r(\mathbf{x}, \mathbf{x}') \right). \quad (\text{S47})$$

In particular, for $i \neq j$ and provided the denominator is positive,

$$\text{Corr}(f_{i,d}(\mathbf{x}), f_{j,d}(\mathbf{x})) = \frac{\kappa_0(\mathbf{x}, \mathbf{x})}{\kappa_0(\mathbf{x}, \mathbf{x}) + \kappa_r(\mathbf{x}, \mathbf{x})} = \frac{\Phi_0(\mathbf{x})\Phi_0(\mathbf{x})^\top}{\Phi_0(\mathbf{x})\Phi_0(\mathbf{x})^\top + \lambda_r^{-1} \Phi_r(\mathbf{x})\Phi_r(\mathbf{x})^\top}. \quad (\text{S48})$$

Proof. Because all coefficient priors are centered, $\mathbb{E}[f_{i,d}(\mathbf{x})] = 0$, so

$$\text{Cov}(f_{i,d}(\mathbf{x}), f_{j,d'}(\mathbf{x}')) = \mathbb{E}[f_{i,d}(\mathbf{x})f_{j,d'}(\mathbf{x}')]. \quad (\text{S49})$$

Expanding both fields gives

$$\begin{aligned} \mathbb{E}[f_{i,d}(\mathbf{x})f_{j,d'}(\mathbf{x}')] &= \mathbb{E}\left[(\Phi_0(\mathbf{x})\mathbf{b}_{0,d} + \Phi_r(\mathbf{x})\mathbf{b}_{i,d})(\Phi_0(\mathbf{x}')\mathbf{b}_{0,d'} + \Phi_r(\mathbf{x}')\mathbf{b}_{j,d'})\right] \\ &= \Phi_0(\mathbf{x})\mathbb{E}[\mathbf{b}_{0,d}\mathbf{b}_{0,d'}^\top]\Phi_0(\mathbf{x}')^\top + \Phi_r(\mathbf{x})\mathbb{E}[\mathbf{b}_{i,d}\mathbf{b}_{j,d'}^\top]\Phi_r(\mathbf{x}')^\top, \end{aligned} \quad (\text{S50})$$

because the cross terms vanish by independence and zero mean. Since the shared coefficients are independent across outputs,

$$\mathbb{E}[\mathbf{b}_{0,d}\mathbf{b}_{0,d'}^\top] = \mathbb{I}\{d = d'\}\mathbf{I}_{l_0}. \quad (\text{S51})$$

Likewise, for the subject-specific coefficients,

$$\mathbb{E}[\mathbf{b}_{i,d}\mathbf{b}_{j,d'}^\top] = \mathbb{I}\{d = d'\}\mathbb{I}\{i = j\}\lambda_r^{-1}\mathbf{I}_{l_r}. \quad (\text{S52})$$

Substituting these identities yields Eq. (S47). For $i \neq j$ and common output d , the covariance at the same input is $\kappa_0(\mathbf{x}, \mathbf{x})$, whereas the marginal variance of each subject field is

$$\text{Var}(f_{i,d}(\mathbf{x})) = \kappa_0(\mathbf{x}, \mathbf{x}) + \kappa_r(\mathbf{x}, \mathbf{x}). \quad (\text{S53})$$

Dividing covariance by the geometric mean of these equal marginal variances gives Eq. (S48). \square

Equation (S48) provides a direct interpretation of the mixed-effect hierarchy: at any fixed state \mathbf{x} , cross-subject correlation is entirely due to the shared field and is damped by the size of the local residual variance.

Proposition 4 (Predictive uncertainty decomposition in field space). *Under the factorized Gaussian posterior*

$$q(\mathbf{b}_{0,d}) = \mathcal{N}(\mathbf{m}_{0,d}, \mathbf{S}_{0,d}), \quad q(\mathbf{b}_{i,d}) = \mathcal{N}(\mathbf{m}_{i,d}, \mathbf{S}_{i,d}), \quad (\text{S54})$$

the latent field value $f_{i,d}(\mathbf{x})$ satisfies

$$f_{i,d}(\mathbf{x}) \mid q \sim \mathcal{N}(\mu_{i,d}^f(\mathbf{x}), v_{i,d}^f(\mathbf{x})), \quad (\text{S55})$$

with

$$\mu_{i,d}^f(\mathbf{x}) = \Phi_0(\mathbf{x})\mathbf{m}_{0,d} + \Phi_r(\mathbf{x})\mathbf{m}_{i,d}, \quad (\text{S56})$$

$$v_{i,d}^f(\mathbf{x}) = v_{i,d}^{\text{pop}}(\mathbf{x}) + v_{i,d}^{\text{loc}}(\mathbf{x}), \quad (\text{S57})$$

where

$$v_{i,d}^{\text{pop}}(\mathbf{x}) := \Phi_0(\mathbf{x})\mathbf{S}_{0,d}\Phi_0(\mathbf{x})^\top, \quad v_{i,d}^{\text{loc}}(\mathbf{x}) := \Phi_r(\mathbf{x})\mathbf{S}_{i,d}\Phi_r(\mathbf{x})^\top. \quad (\text{S58})$$

A natural pointwise diagnostic is the local uncertainty fraction

$$\rho_{i,d}^{\text{loc}}(\mathbf{x}) := \frac{v_{i,d}^{\text{loc}}(\mathbf{x})}{v_{i,d}^{\text{pop}}(\mathbf{x}) + v_{i,d}^{\text{loc}}(\mathbf{x})}, \quad \rho_{i,d}^{\text{pop}}(\mathbf{x}) = 1 - \rho_{i,d}^{\text{loc}}(\mathbf{x}). \quad (\text{S59})$$

Proof. The field value is an affine function of two independent Gaussian coefficient vectors,

$$f_{i,d}(\mathbf{x}) = \Phi_0(\mathbf{x})\mathbf{b}_{0,d} + \Phi_r(\mathbf{x})\mathbf{b}_{i,d}, \quad (\text{S60})$$

so it is Gaussian under q . Its mean is obtained by linearity of expectation, its variance is the sum of the two quadratic forms because the posterior is factorized between shared and local coefficients. \square

The additive variance decomposition in Proposition 4 is exact at fixed state inputs. After pushing uncertainty through the nonlinear ODE solution map, the analogous decomposition is no longer additive in general, but an exact law-of-total-variance identity remains available.

Proposition 5 (Exact trajectory-space variance decomposition). *For each subject i , let*

$$\mathbf{B}_0 := (\mathbf{b}_{0,1}^\top, \dots, \mathbf{b}_{0,D}^\top)^\top \in \mathbb{R}^{Dl_0}, \quad \mathbf{B}_i := (\mathbf{b}_{i,1}^\top, \dots, \mathbf{b}_{i,D}^\top)^\top \in \mathbb{R}^{Dl_r}, \quad (\text{S61})$$

and let $\mathbf{x}_i(\cdot; \mathbf{B}_0, \mathbf{B}_i, \mathbf{x}_i^)$ denote the trajectory obtained by integrating the subject-specific field from initial condition \mathbf{x}_i^* . For any square-integrable trajectory functional*

$$\mathcal{H}_i = \mathcal{H}(\mathbf{x}_i(\cdot; \mathbf{B}_0, \mathbf{B}_i, \mathbf{x}_i^*)),$$

the posterior variance satisfies

$$\text{Var}_q(\mathcal{H}_i) = \text{Var}_q(\mathbf{B}_0) \left(\mathbb{E}_{q(\mathbf{B}_i)}[\mathcal{H}_i \mid \mathbf{B}_0] \right) + \mathbb{E}_{q(\mathbf{B}_0)} \left[\text{Var}_{q(\mathbf{B}_i)}(\mathcal{H}_i \mid \mathbf{B}_0) \right]. \quad (\text{S62})$$

A natural trajectory-level analogue of Eq. (S59) is therefore

$$\rho_i^{\text{loc}}[\mathcal{H}] := \frac{\mathbb{E}_{q(\mathbf{B}_0)}[\text{Var}_{q(\mathbf{B}_i)}(\mathcal{H}_i \mid \mathbf{B}_0)]}{\text{Var}_q(\mathcal{H}_i)}, \quad \rho_i^{\text{pop}}[\mathcal{H}] = 1 - \rho_i^{\text{loc}}[\mathcal{H}]. \quad (\text{S63})$$

This applies in particular to pointwise trajectory coordinates $\mathcal{H}_i = e_a^\top \mathbf{x}_i(t)$ and final-state summaries.

Proof. Equation (S62) is the law of total variance with conditioning variable \mathbf{B}_0 and inner randomness coming from \mathbf{B}_i . \square

For computation, it is useful to complement the exact identity above with a first-order pushforward approximation. Let

$$\mathbf{M}_0 := \mathbb{E}_q[\mathbf{B}_0], \quad \mathbf{M}_i := \mathbb{E}_q[\mathbf{B}_i], \quad (\text{S64})$$

and let

$$\boldsymbol{\Sigma}_{\mathbf{B}_0} := \text{blockdiag}(\mathbf{S}_{0,1}, \dots, \mathbf{S}_{0,D}) \in \mathbb{R}^{Dl_0 \times Dl_0}, \quad \boldsymbol{\Sigma}_{\mathbf{B}_i} := \text{blockdiag}(\mathbf{S}_{i,1}, \dots, \mathbf{S}_{i,D}) \in \mathbb{R}^{Dl_r \times Dl_r}. \quad (\text{S65})$$

For a fixed time t and coordinate a , define the solution map

$$\psi_{i,a,t} : \mathbb{R}^{Dl_0} \times \mathbb{R}^{Dl_r} \rightarrow \mathbb{R}, \quad \psi_{i,a,t}(\mathbf{B}_0, \mathbf{B}_i) := e_a^\top \mathbf{x}_i(t; \mathbf{B}_0, \mathbf{B}_i, \mathbf{x}_i^*), \quad (\text{S66})$$

and its sensitivity rows at the posterior mean,

$$\mathbf{J}_{0,i,a}(t) := \nabla_{\mathbf{B}_0} \psi_{i,a,t}(\mathbf{M}_0, \mathbf{M}_i) \in \mathbb{R}^{1 \times Dl_0}, \quad \mathbf{J}_{r,i,a}(t) := \nabla_{\mathbf{B}_i} \psi_{i,a,t}(\mathbf{M}_0, \mathbf{M}_i) \in \mathbb{R}^{1 \times Dl_r}. \quad (\text{S67})$$

Then the first-order approximation

$$\psi_{i,a,t}(\mathbf{B}_0, \mathbf{B}_i) \approx \psi_{i,a,t}(\mathbf{M}_0, \mathbf{M}_i) + \mathbf{J}_{0,i,a}(t)(\mathbf{B}_0 - \mathbf{M}_0) + \mathbf{J}_{r,i,a}(t)(\mathbf{B}_i - \mathbf{M}_i) \quad (\text{S68})$$

yields the additive variance approximation

$$\text{Var}_q(e_a^\top \mathbf{x}_i(t)) \approx \mathbf{J}_{0,i,a}(t) \boldsymbol{\Sigma}_{\mathbf{B}_0} \mathbf{J}_{0,i,a}(t)^\top + \mathbf{J}_{r,i,a}(t) \boldsymbol{\Sigma}_{\mathbf{B}_i} \mathbf{J}_{r,i,a}(t)^\top. \quad (\text{S69})$$

This gives a computable pointwise trajectory analogue of Eq. (S59):

$$\rho_{i,a}^{\text{loc}}(t) \approx \frac{\mathbf{J}_{r,i,a}(t) \boldsymbol{\Sigma}_{\mathbf{B}_i} \mathbf{J}_{r,i,a}(t)^\top}{\mathbf{J}_{0,i,a}(t) \boldsymbol{\Sigma}_{\mathbf{B}_0} \mathbf{J}_{0,i,a}(t)^\top + \mathbf{J}_{r,i,a}(t) \boldsymbol{\Sigma}_{\mathbf{B}_i} \mathbf{J}_{r,i,a}(t)^\top}. \quad (\text{S70})$$

E.3 The conditional field update as weighted mixed ridge regression

The remaining statements are exact for the Gaussian field subproblem obtained once the current smoothed pseudo-derivatives are fixed. In that regime, the field update is exactly a weighted mixed ridge regression.

Fix an output dimension d , and consider the pseudo-regression model of Section 3.4,

$$\mathbf{u}_{i,d} = \mathbf{P}_{0,i,d} \mathbf{b}_{0,d} + \mathbf{P}_{r,i,d} \mathbf{b}_{i,d} + \boldsymbol{\varepsilon}_{i,d}^{\text{reg}}, \quad \boldsymbol{\varepsilon}_{i,d}^{\text{reg}} \sim \mathcal{N}(\mathbf{0}, \mathbf{R}_{i,d}). \quad (\text{S71})$$

Introduce the stacked coefficient vector

$$\boldsymbol{\beta}_d := (\mathbf{b}_{0,d}^\top, \mathbf{b}_{1,d}^\top, \dots, \mathbf{b}_{M,d}^\top)^\top \in \mathbb{R}^{l_0 + Ml_r}. \quad (\text{S72})$$

and the block-diagonal prior precision

$$\mathbf{\Omega}_d := \text{blockdiag}(\mathbf{I}_{l_0}, \lambda_r \mathbf{I}_{l_r}, \dots, \lambda_r \mathbf{I}_{l_r}) \in \mathbb{R}^{(l_0 + Ml_r) \times (l_0 + Ml_r)}. \quad (\text{S73})$$

For each subject i , let $\mathbf{A}_{i,d}$ denote the block row that injects $\mathbf{P}_{0,i,d}$ in the shared block and $\mathbf{P}_{r,i,d}$ in the i th local block:

$$\mathbf{A}_{i,d} = [\mathbf{P}_{0,i,d} \ \mathbf{0} \ \cdots \ \mathbf{0} \ \mathbf{P}_{r,i,d} \ \mathbf{0} \ \cdots \ \mathbf{0}] \in \mathbb{R}^{(K_i+1) \times (l_0 + Ml_r)}. \quad (\text{S74})$$

Then the joint pseudo-regression model reads

$$\mathbf{u}_{i,d} = \mathbf{A}_{i,d} \boldsymbol{\beta}_d + \boldsymbol{\varepsilon}_{i,d}^{\text{reg}}. \quad (\text{S75})$$

Proposition 6 (Exact weighted mixed-ridge form). *Conditionally on the smoothed pseudo-data, the joint posterior over $\boldsymbol{\beta}_d$ is Gaussian and satisfies*

$$p(\boldsymbol{\beta}_d \mid \{\mathbf{u}_{i,d}\}_{i=1}^M) \propto \exp(-\mathcal{J}_d(\boldsymbol{\beta}_d)), \quad (\text{S76})$$

where, up to an additive constant,

$$\mathcal{J}_d(\boldsymbol{\beta}_d) = \frac{1}{2} \sum_{i=1}^M \left\| \mathbf{R}_{i,d}^{-1/2} (\mathbf{u}_{i,d} - \mathbf{A}_{i,d} \boldsymbol{\beta}_d) \right\|^2 + \frac{1}{2} \boldsymbol{\beta}_d^\top \mathbf{\Omega}_d \boldsymbol{\beta}_d. \quad (\text{S77})$$

Equivalently, in block form,

$$\mathcal{J}_d(\mathbf{b}_{0,d}, \{\mathbf{b}_{i,d}\}) = \frac{1}{2} \sum_{i=1}^M \left\| \mathbf{R}_{i,d}^{-1/2} (\mathbf{u}_{i,d} - \mathbf{P}_{0,i,d} \mathbf{b}_{0,d} - \mathbf{P}_{r,i,d} \mathbf{b}_{i,d}) \right\|^2 + \frac{1}{2} \|\mathbf{b}_{0,d}\|^2 + \frac{\lambda_r}{2} \sum_{i=1}^M \|\mathbf{b}_{i,d}\|^2. \quad (\text{S78})$$

Thus the field update is exactly a weighted mixed ridge regression in feature space.

Proof. The pseudo-likelihood is Gaussian:

$$p(\{\mathbf{u}_{i,d}\} \mid \boldsymbol{\beta}_d) \propto \prod_{i=1}^M \exp\left(-\frac{1}{2} (\mathbf{u}_{i,d} - \mathbf{A}_{i,d} \boldsymbol{\beta}_d)^\top \mathbf{R}_{i,d}^{-1} (\mathbf{u}_{i,d} - \mathbf{A}_{i,d} \boldsymbol{\beta}_d)\right). \quad (\text{S79})$$

The Gaussian priors on the shared and local coefficients contribute the quadratic penalty

$$p(\boldsymbol{\beta}_d) \propto \exp\left(-\frac{1}{2} \boldsymbol{\beta}_d^\top \mathbf{\Omega}_d \boldsymbol{\beta}_d\right). \quad (\text{S80})$$

Multiplying prior and likelihood and taking the negative logarithm yields Eq. (S77). Expanding the block structure of $\mathbf{A}_{i,d}$ yields Eq. (S78). Since both prior and likelihood are Gaussian, the posterior is Gaussian. \square

Because $\mathbf{\Omega}_d \succ 0$, the objective above is strictly convex.

Corollary 7 (Joint and conditional uniqueness). *For each output dimension d , the objective \mathcal{J}_d in Eq. (S77) has a unique global minimizer. Moreover, if all blocks except one are held fixed, the corresponding block subproblem is again strictly convex and has a unique minimizer.*

Proof. The Hessian of \mathcal{J}_d is

$$\nabla^2 \mathcal{J}_d = \mathbf{\Omega}_d + \sum_{i=1}^M \mathbf{A}_{i,d}^\top \mathbf{R}_{i,d}^{-1} \mathbf{A}_{i,d}. \quad (\text{S81})$$

The first term is strictly positive definite because the shared prior precision is \mathbf{I}_{l_0} and each local prior precision is $\lambda_r \mathbf{I}_{l_r}$ with $\lambda_r > 0$. The second term is positive semidefinite. Hence $\nabla^2 \mathcal{J}_d \succ 0$, so \mathcal{J}_d is strictly convex and has a unique global minimizer. Restricting to any one block while holding the others fixed leaves a strictly positive definite block Hessian, and the corresponding block subproblem is therefore strictly convex as well. \square

The natural-parameter updates in the main text are precisely the normal equations of these block subproblems.

Corollary 8 (Equivalence with the natural-parameter updates). *Fix an output dimension d .*

- If $\mathbf{b}_{1,d}, \dots, \mathbf{b}_{M,d}$ are held fixed, then the unique minimizer in $\mathbf{b}_{0,d}$ satisfies

$$\left(\mathbf{I}_{l_0} + \sum_{i=1}^M \mathbf{P}_{0,i,d}^\top \mathbf{R}_{i,d}^{-1} \mathbf{P}_{0,i,d} \right) \mathbf{b}_{0,d} = \sum_{i=1}^M \mathbf{P}_{0,i,d}^\top \mathbf{R}_{i,d}^{-1} (\mathbf{u}_{i,d} - \mathbf{P}_{r,i,d} \mathbf{b}_{i,d}). \quad (\text{S82})$$

- If $\mathbf{b}_{0,d}$ is held fixed, then the unique minimizer in $\mathbf{b}_{i,d}$ satisfies

$$\left(\lambda_r \mathbf{I}_{l_r} + \mathbf{P}_{r,i,d}^\top \mathbf{R}_{i,d}^{-1} \mathbf{P}_{r,i,d} \right) \mathbf{b}_{i,d} = \mathbf{P}_{r,i,d}^\top \mathbf{R}_{i,d}^{-1} (\mathbf{u}_{i,d} - \mathbf{P}_{0,i,d} \mathbf{b}_{0,d}). \quad (\text{S83})$$

If the complementary blocks are replaced by their current posterior means $\mathbf{m}_{i,d}$ and $\mathbf{m}_{0,d}$, these equations coincide exactly with Eqs. (25)–(28) in the main text. In particular, the natural-parameter updates are simply the precision-form representation of the corresponding weighted mixed-ridge solutions.

Proof. Differentiate Eq. (S78) with respect to the relevant block, set the gradient to zero, and identify the resulting normal equations. Since each block conditional posterior is Gaussian, its precision-form parameters are exactly the left-hand-side matrix and right-hand-side vector appearing in these normal equations. \square

E.4 Spectral shrinkage and effective degrees of freedom

The local field update admits a spectral interpretation that makes the role of λ_r and the amount of subject-specific adaptation interpretable.

Fix a subject i and output dimension d , and define the residualized pseudo-target

$$\mathbf{r}_{i,d} := \mathbf{u}_{i,d} - \mathbf{P}_{0,i,d} \mathbf{m}_{0,d}. \quad (\text{S84})$$

The local posterior mean in the main text is

$$\mathbf{m}_{i,d} = \left(\lambda_r \mathbf{I}_{l_r} + \mathbf{P}_{r,i,d}^\top \mathbf{R}_{i,d}^{-1} \mathbf{P}_{r,i,d} \right)^{-1} \mathbf{P}_{r,i,d}^\top \mathbf{R}_{i,d}^{-1} \mathbf{r}_{i,d}. \quad (\text{S85})$$

Proposition 9 (Spectral shrinkage form of the local update). *Let*

$$\mathbf{R}_{i,d}^{-1/2} \mathbf{P}_{r,i,d} = \mathbf{U}_{i,d} \text{diag}(\sigma_{i,d,1}, \dots, \sigma_{i,d,J_{i,d}}) \mathbf{V}_{i,d}^\top \quad (\text{S86})$$

be a compact singular value decomposition, where $J_{i,d} = \text{rank}(\mathbf{R}_{i,d}^{-1/2} \mathbf{P}_{r,i,d})$ and the index $j = 1, \dots, J_{i,d}$ runs over weighted singular directions of the subject-specific design matrix. Then

$$\mathbf{m}_{i,d} = \mathbf{V}_{i,d} \text{diag} \left(\frac{\sigma_{i,d,j}}{\lambda_r + \sigma_{i,d,j}^2} \right)_{j=1}^{J_{i,d}} \mathbf{U}_{i,d}^\top \mathbf{R}_{i,d}^{-1/2} \mathbf{r}_{i,d}, \quad (\text{S87})$$

and the fitted local contribution satisfies

$$\mathbf{P}_{r,i,d} \mathbf{m}_{i,d} = \mathbf{R}_{i,d}^{1/2} \mathbf{U}_{i,d} \text{diag}(\alpha_{i,d,j})_{j=1}^{J_{i,d}} \mathbf{U}_{i,d}^\top \mathbf{R}_{i,d}^{-1/2} \mathbf{r}_{i,d}, \quad \alpha_{i,d,j} := \frac{\sigma_{i,d,j}^2}{\lambda_r + \sigma_{i,d,j}^2}. \quad (\text{S88})$$

Thus each weighted singular direction is retained with shrinkage factor $\alpha_{i,d,j} \in [0, 1)$.

Proof. Substitute the compact singular value decomposition into Eq. (S85):

$$\begin{aligned} \mathbf{m}_{i,d} &= (\lambda_r \mathbf{I}_{l_r} + \mathbf{V}_{i,d} \text{diag}(\sigma_{i,d,j}^2) \mathbf{V}_{i,d}^\top)^{-1} \mathbf{V}_{i,d} \text{diag}(\sigma_{i,d,j}) \mathbf{U}_{i,d}^\top \mathbf{R}_{i,d}^{-1/2} \mathbf{r}_{i,d} \\ &= \mathbf{V}_{i,d} \text{diag} \left(\frac{\sigma_{i,d,j}}{\lambda_r + \sigma_{i,d,j}^2} \right) \mathbf{U}_{i,d}^\top \mathbf{R}_{i,d}^{-1/2} \mathbf{r}_{i,d}, \end{aligned} \quad (\text{S89})$$

which is Eq. (S87). Multiplying by $\mathbf{P}_{r,i,d} = \mathbf{R}_{i,d}^{1/2} \mathbf{U}_{i,d} \text{diag}(\sigma_{i,d,j}) \mathbf{V}_{i,d}^\top$ yields Eq. (S88). \square

Proposition 9 shows that subject-specific personalization is strongest along directions that are both well supported by the pseudo-data and weakly penalized by λ_r . A natural scalar summary is the effective number of local degrees of freedom

$$\text{df}_{i,d}^{\text{loc}} := \sum_{j=1}^{J_{i,d}} \frac{\sigma_{i,d,j}^2}{\lambda_r + \sigma_{i,d,j}^2}. \quad (\text{S90})$$

This quantity lies between 0 and $J_{i,d}$ and measures how much local flexibility is effectively used for subject i and output d .

E.5 Monotone information accumulation

The shared-field update aggregates information across subjects by summing positive semidefinite contributions. This gives a simple monotonicity property that mirrors the common-mean Gaussian-process updates of MAGMA [19]: adding subjects can only increase shared precision and decrease shared posterior covariance.

Proposition 10 (Monotone accumulation of information). *Fix an output dimension d and consider the shared precision update*

$$\mathbf{\Lambda}_{0,d}^{(M)} := \mathbf{I}_{l_0} + \sum_{i=1}^M \mathbf{P}_{0,i,d}^\top \mathbf{R}_{i,d}^{-1} \mathbf{P}_{0,i,d}. \quad (\text{S91})$$

Then

$$\mathbf{\Lambda}_{0,d}^{(M+1)} - \mathbf{\Lambda}_{0,d}^{(M)} = \mathbf{P}_{0,M+1,d}^\top \mathbf{R}_{M+1,d}^{-1} \mathbf{P}_{0,M+1,d} \succeq \mathbf{0}. \quad (\text{S92})$$

Consequently, the corresponding posterior covariances satisfy

$$\left(\mathbf{\Lambda}_{0,d}^{(M+1)}\right)^{-1} \preceq \left(\mathbf{\Lambda}_{0,d}^{(M)}\right)^{-1}. \quad (\text{S93})$$

An analogous statement holds for the local precision of a fixed subject when additional pseudo-derivative observations are added to that subject.

Proof. Equation (S92) is immediate because $\mathbf{R}_{M+1,d}^{-1} \succ \mathbf{0}$, so the quadratic form $\mathbf{P}_{0,M+1,d}^\top \mathbf{R}_{M+1,d}^{-1} \mathbf{P}_{0,M+1,d}$ is positive semidefinite. The covariance monotonicity then follows from the order-reversing property of matrix inversion on the cone of symmetric positive definite matrices. The local statement is identical. \square

This algebraic structure is closely related to the common-mean multi-task GP update used in MAGMA [19], where the shared precision likewise accumulates a sum of task-specific positive semidefinite contributions. The difference here is that the contributions arise from ODE-induced pseudo-derivative regressions rather than directly from observed outputs.

The same monotonicity extends to trajectory summaries under the first-order pushforward approximation of Eq. (S69). Indeed, if $\mathbf{\Sigma}_{B_0}^{(M+1)} \preceq \mathbf{\Sigma}_{B_0}^{(M)}$, then for any fixed sensitivity row $\mathbf{J}_{0,i,a}(t)$,

$$\mathbf{J}_{0,i,a}(t) \mathbf{\Sigma}_{B_0}^{(M+1)} \mathbf{J}_{0,i,a}(t)^\top \leq \mathbf{J}_{0,i,a}(t) \mathbf{\Sigma}_{B_0}^{(M)} \mathbf{J}_{0,i,a}(t)^\top. \quad (\text{S94})$$

Thus, at least at the linearized level, adding subjects can only reduce the population-driven component of trajectory uncertainty.

F Alternative scalable vector field approximations

Although the main text uses inducing-feature representations for the shared and subject-specific vector fields, the overall framework is compatible with other scalable GP approximations. The main requirement is that, at fixed inputs, the field admits a linear-Gaussian representation in a finite set of coefficients.

Consider the generic construction

$$f_{0,d}(\mathbf{x}) = \varphi_0(\mathbf{x})^\top \mathbf{b}_{0,d}, \quad g_{i,d}(\mathbf{x}) = \varphi_r(\mathbf{x})^\top \mathbf{b}_{i,d}, \quad f_{i,d}(\mathbf{x}) = f_{0,d}(\mathbf{x}) + g_{i,d}(\mathbf{x}), \quad (\text{S95})$$

with feature maps $\varphi_0 : \mathbb{R}^D \rightarrow \mathbb{R}^{L_0}$ and $\varphi_r : \mathbb{R}^D \rightarrow \mathbb{R}^{L_r}$, and Gaussian priors

$$\mathbf{b}_{0,d} \sim \mathcal{N}(\mathbf{0}, \mathbf{\Omega}_0^{-1}), \quad \mathbf{b}_{i,d} \sim \mathcal{N}(\mathbf{0}, \mathbf{\Omega}_r^{-1}). \quad (\text{S96})$$

If the approximate posteriors remain Gaussian,

$$q(\mathbf{b}_{0,d}) = \mathcal{N}(\mathbf{m}_{0,d}, \mathbf{S}_{0,d}), \quad q(\mathbf{b}_{i,d}) = \mathcal{N}(\mathbf{m}_{i,d}, \mathbf{S}_{i,d}),$$

then field moments are still available in closed form:

$$\mu_{i,d}^f(\mathbf{x}) = \varphi_0(\mathbf{x})^\top \mathbf{m}_{0,d} + \varphi_r(\mathbf{x})^\top \mathbf{m}_{i,d}, \quad (\text{S97})$$

$$v_{i,d}^f(\mathbf{x}) = \varphi_0(\mathbf{x})^\top \mathbf{S}_{0,d} \varphi_0(\mathbf{x}) + \varphi_r(\mathbf{x})^\top \mathbf{S}_{i,d} \varphi_r(\mathbf{x}). \quad (\text{S98})$$

Whenever the feature maps are differentiable, the Jacobian of the posterior-mean field is explicit as well:

$$\nabla_{\mathbf{x}} \mathbb{E}_q[f_{i,d}(\mathbf{x})] = \nabla_{\mathbf{x}} \varphi_0(\mathbf{x})^\top \mathbf{m}_{0,d} + \nabla_{\mathbf{x}} \varphi_r(\mathbf{x})^\top \mathbf{m}_{i,d}. \quad (\text{S99})$$

This is sufficient for the trajectory-space linearization. On the field side, once the smoothed pseudo-derivatives are available, the update remains a Gaussian mixed regression problem with the same form as in Section 3.4, except that the identity prior precisions are replaced by $\mathbf{\Omega}_0$ and $\mathbf{\Omega}_r$. The inducing-feature construction used in the main text is recovered by taking $\varphi_0 = \Phi_0$, $\varphi_r = \Phi_r$, and whitened priors.

This yields two alternatives.

Random Fourier features. For stationary kernels, one may replace inducing features by random Fourier features [29]. In that case, φ_0 and φ_r are finite-dimensional random feature maps, and the model remains exactly in the form of Eq. (S95). This yields the same alternating algorithm. The main advantages are simplicity, fast dense linear algebra, and tunable capacities through L_0 and L_r ; the main drawback is that random features do not adapt to the observed state distribution, so many features may be needed when the field has localized structure.

Hilbert basis expansions. On a bounded state domain, one may instead use Hilbert or spectral basis-function approximations [35]. Then φ_0 and φ_r are deterministic basis expansions, for example built from Laplace eigenfunctions with appropriate spectral weights. This again preserves the linear-Gaussian field layer and therefore leaves the trajectory update and mixed-regression field update unchanged. The main advantages are a deterministic low-rank representation and explicit control of spectral structure; the main limitation is that one must choose a suitable bounded state domain and basis, which may be less flexible when the relevant state region is not known in advance.